HHS Public Access

Author manuscript

Nat Immunol. Author manuscript; available in PMC 2025 January 02.

Published in final edited form as:

Nat Immunol. 2024 January ; 25(1): 66–76. doi:10.1038/s41590-023-01682-z.

CD4+ T cell immunity is dependent on an intrinsic stem-like program

Dawei Zou[1,2], **Zheng Yin**[3,4], **Stephanie G. Yi**[5,6], **Guohua Wang**[1], **Yang Guo**[1], **Xiang Xiao**[1], **Shuang Li**[7], **Xiaolong Zhang**[1], **Nancy M. Gonzalez**[1], **Laurie J. Minze**[1], **Lin Wang**[3], **Stephen T. C. Wong**[3,4], **A. Osama Gaber**[5,6], **Rafik M. Ghobrial**[5,6], **Xian C. Li**[1,6], **Wenhao Chen**[1,6,✉]

[1]Immunobiology & Transplant Science Center, Department of Surgery, Houston Methodist Research Institute, Houston Methodist Hospital, Houston, TX, USA.

[2]Organ Transplant Center, The First Affiliated Hospital, Sun Yat-sen University, Guangzhou, China.

[3]Systems Medicine and Bioengineering Department, Houston Methodist Neal Cancer Center, Houston, TX, USA.

[4]Department of Radiology, Houston Methodist Hospital, Weill Cornell Medicine, Houston, TX, USA.

[5]Department of Surgery, J. C. Walter Jr. Transplant Center, Houston Methodist Hospital, Houston, TX, USA.

[6]Department of Surgery, Weill Cornell Medicine, Cornell University, New York, NY, USA.

[7]Center for Neuroregeneration, Houston Methodist Research Institute, Houston, TX, USA.

Abstract

CD4+ T cells are central to various immune responses, but the molecular programs that drive and maintain CD4+ T cell immunity are not entirely clear. Here we identify a stem-like program that

✉**Correspondence and requests for materials** should be addressed to Wenhao Chen. wchen@houstonmethodist.org.

Author contributions

D.Z., X.X., X.C.L. and W.C. designed the study and wrote the manuscript. D.Z., Z.Y. and W.C. performed core experimental work and data analysis. Z.Y., L.W. and S.T.C.W. performed computational analyses. S.G.Y., G.W., Y.G., S.L., X.Z., N.M.G., L.J.M., A.O.G. and R.M.G. performed supporting experimental work and data analysis.

Competing interests

The authors declare no competing interests.

Additional information

Extended data is available for this paper at https://doi.org/10.1038/s41590-023-01682-z.

Supplementary information The online version contains supplementary material available at https://doi.org/10.1038/s41590-023-01682-z.

Peer review information *Nature Immunology* thanks Vijay Kuchroo and the other, anonymous, reviewer(s) for their contribution to the peer review of this work. Primary Handling Editor: N. Bernard, in collaboration with the *Nature Immunology* team. Peer reviewer reports are available.

Reporting summary

Further information on research design is available in the Nature Portfolio Reporting Summary linked to this article.

Code availability

ScRNA-seq data analyses were conducted using publicly available codes and open-source software packages. No new algorithms were developed for this study.

governs the $CD4^+$ T cell response in transplantation models. Single-cell-transcriptomic analysis revealed that naive alloantigen-specific $CD4^+$ T cells develop into $TCF1^{hi}$ effector precursor (T_{EP}) cells and $TCF1^-CXCR6^+$ effectors in transplant recipients. The $TCF1^-CXCR6^+CD4^+$ effectors lose proliferation capacity and do not reject allografts upon adoptive transfer into secondary hosts. By contrast, the $TCF1^{hi}CD4^+$ T_{EP} cells have dual features of self-renewal and effector differentiation potential, and allograft rejection depends on continuous replenishment of $TCF1^-CXCR6^+$ effectors from $TCF1^{hi}CD4^+$ T_{EP} cells. Mechanistically, TCF1 sustains the $CD4^+$ T_{EP} cell population, whereas the transcription factor IRF4 and the glycolytic enzyme LDHA govern the effector differentiation potential of $CD4^+$ T_{EP} cells. Deletion of IRF4 or LDHA in T cells induces transplant acceptance. These findings unravel a stem-like program that controls the self-renewal capacity and effector differentiation potential of $CD4^+$ T_{EP} cells and have implications for T cell- related immunotherapies.

$CD4^+$ T cells have a central function in adaptive immunity. Upon antigen encounter, naive $CD4^+$ T cells are activated and then differentiate into various effector helper T (T_H) cell subsets[1,2]. While the initial events and molecular pathways leading to T cell activation have been studied extensively[3], the mechanisms that maintain the subsequent $CD4^+$ T cell effector programs are not completely clear. The identification of antigen-primed 'stem-like' $CD4^+$ T cells is a recent advance in this field. For instance, in a multiple sclerosis model, stem-like $TCF1^+SLAMF6$ $(Ly108)^+$ T_H17 cells have been identified as precursor cells that give rise to encephalitogenic $GM\text{-}CSF^+IFN\text{-}\gamma^+CXCR6^+$ effector T cells. In addition to residing in multiple lymphoid organs, these stem-like T_H17 cells also migrate to the intestine, where they are sustained by the gut microbiota[4]. In a chronic infection model, antigen-primed $TCF1^+CD4^+$ T cells have been identified as precursor cells for both effector T cells and follicular helper T (T_{FH}) cells[5]. These studies highlight the stem-like features of $TCF1^+CD4^+$ T_{EP} cells, characterized by their capacity for self-renewal and potential for subsequent effector differentiation. Further research is needed to determine whether these two features are controlled by distinct intrinsic programs, and to what extent they impact $CD4^+$ T cell response.

The transcription factor TCF1 plays a critical role in various aspects of T cell biology, including thymic development, the differentiation of T_{FH} cells and the generation of memory T cells[6–8]. Additionally, TCF1 promotes the self-renewal of stem-like $CD8^+$ T cells, also known as precursors of exhausted T cells, particularly in the context of chronic infections[9–11]. TCF1's expression is abundant in naive T cells and continues to persist in stem-like T cells following antigen stimulation; however, its expression is downregulated in terminally differentiated effector and exhausted T cells[10–12]. In contrast, the transcription factor IRF4 is usually absent in naive T cells. Upon activation, IRF4 expression is rapidly induced in T cells, and the level of expression directly correlates with the strength of the T cell receptor (TCR) signal[13]. IRF4 is necessary for the differentiation of T_H2, T_H9, T_H17, T_{FH}, and cytotoxic effector $CD8^+$ T cells[14–18].

Upon activation and proliferation, T cells substantially increase their glucose uptake and can metabolize glucose into lactate even under oxygen-rich conditions, a phenomenon referred to as aerobic glycolysis or the Warburg effect[19,20]. The enzyme lactate dehydrogenase A

(LDHA) plays a pivotal role in this process, catalyzing the conversion of pyruvate, a glucose metabolite, into lactate[21]. While a deficiency in LDHA has minimal impact on T cell thymic development and T cell homeostasis, it significantly impairs the differentiation of T_H1, T_H17 and cytotoxic effector $CD8^+$ T cells[22–24]. On the other hand, regulatory T cells utilize the transcription factor Foxp3 to downregulate glycolysis[25]. Notably, a recent study has uncovered metabolic similarities between non-pathogenic T_H17 cells and regulatory T cells, whereas pathogenic T_H17 cells exhibit increased aerobic glycolysis and dependency on the polyamine pathway[26].

In experimental organ transplantation, $CD4^+$ T cells are necessary for mediating the rejection of heart and kidney allografts[27–29]. Among the subsets of $CD4^+$ T cells, T_H1 cells have been implicated in causing transplant damage directly through cytotoxicity or by enhancing the activity of macrophages and $CD8^+$ T cells[30]. T_{FH} cells contribute to transplant rejection by promoting the B cell and alloantibody responses[31,32]. Conversely, regulatory T cells provide a protective mechanism against transplant rejection[33,34]; however, it is unknown whether $CD4^+$ T_{EP} cells play a role in transplant rejection and how their stem-like features are regulated at the molecular level.

Here we identify stem-like $TCF1^+Ly108^+CD4^+$ T_{EP} cells in transplant recipients. These cells proliferate extensively before differentiating into $TCF1^-CXCR6^+$ effector cells. While TCF1 supports the self-renewal of $CD4^+$ T_{EP} cells, IRF4 and LDHA govern their effector differentiation potential. In the absence of IRF4 or LDHA, $CD4^+$ T_{EP} cells are unable to differentiate into $TCF1^-CXCR6^+$ effector cells, thereby leading to transplant acceptance; however, $TCF1^-CXCR6^+$ effector cells, while crucial for transplant rejection, lose their proliferative ability and do not persist. This necessitates the continuous differentiation of stem-like T_{EP} cells into effector cells to drive transplant rejection. These findings uncover an intrinsic stem-like program of $CD4^+$ T_{EP} cells in the transplantation context. This mechanism might also extend to other $CD4^+$ T cell-mediated immune responses.

Results

Single-cell transcriptome of alloreactive $CD4^+$ T cells

To determine the overall $CD4^+$ T cell response to transplant antigens, we performed single-cell RNA sequencing (scRNA-seq) of alloantigen-specific $CD4^+$ T cells in transplant recipients. C57BL/6 (B6) mice were adoptively transferred with naive $CD4^+$ TEa transgenic T cells (TCR Vα2Vβ6, B6 background) that recognize an I-E$\alpha_{52–68}$ major alloantigen from BALB/c mice. This alloantigen is presented by $I\text{-}A^b$ molecules on the antigen-presenting cells of the B6 recipients[29,35–37]. One day later, mice were transplanted with BALB/c hearts. Allografts were rejected 7–9 d post-transplantation (Extended Data Fig. 1a). TEa cells from spleens and heart allografts were obtained at 7 d post-transplantation for scRNA-seq (Fig. 1a and Extended Data Fig. 1b). Clustering analysis identified two major stem-like T_{EP} cell clusters of TEa cells in spleens (clusters 0 and 2), marked by high expression of *Tcf7* (encoding TCF1)[9], *Slamf6* (encoding Ly108)[4,38], *Klf2*, *Id3*, *Lef1*, *Sell* and *Ccr7*. The major effector cluster of TEa cells in heart allografts (cluster 1) was marked by high expression of *Cxcr6* (refs. 4,39), *Tnfrsf18* (encoding GITR), *Tnfrsf4*, *Hif1a*, *Nkg7* (ref. 40), *Gzmb*, *Ctla4* and *Pdcd1* (Fig. 1b–d and Extended Data Fig. 1c,d). Clusters 3 and 4 represented

intermediate cell states in allografts and spleens, respectively. Minor clusters 5 to 7 represented proliferating, mitochondrial transcript (MT)-enriched and interferon-stimulated gene (ISG)-enriched TEa cells, respectively (Fig. 1b,c). Notably, the effector TEa cells expressed T_H1 cell genes *Tbx21* and *Ifng*, whereas they showed minimal expression of *Foxp3*, *Tgfb1*, *Il4*, *Il13*, *Il17a* and *Il17f* (Extended Data Fig. 1e).

We used flow cytometry to validate some of the scRNA-seq data. Naive TEa cells were $TCF1^+$ but barely expressed the stem-like precursor marker Ly108. At 7 d post-heart transplantation, most adoptively transferred TEa cells in spleens were $TCF1^{hi}Ly108^{hi}$ stem-like T_{EP} cells and approximately 60% graft-infiltrating TEa cells downregulated the expression of TCF1 and Ly108. Moreover, graft-infiltrating but not splenic TEa cells expressed high levels of CXCR6 and GITR (Fig. 1e). Collectively, naive alloantigen-specific $CD4^+$ T cells mainly develop into $TCF1^{hi}Ly108^{hi}$ T_{EP} cells and $TCF1^-CXCR6^+$ effectors in response to heart transplantation.

Transfer of $CD4^+$ T_{EP} but not effector cells induces graft rejection

To demonstrate the impact of $TCF1^{hi}CD4^+$ T_{EP} cells on transplant survival, we used a *Tcf7*^{GFP} reporter system to isolate live $TCF1^{hi}$ and $TCF1^-CD4^+$ T cells. B6.*Tcf7*^{GFP} reporter mice rejected BALB/c hearts at a rate comparable to wild-type (WT) B6 mice (Extended Data Fig. 2a,b). At 7 d post-heart transplantation, $TCF1^{hi}$ and $TCF1^-$ cells were isolated from the antigen-experienced $CD4^+CD44^+$ splenocytes and adoptively transferred into B6.*Rag1*$^{-/-}$ mice (Fig. 2a,b). One day later, *Rag1*$^{-/-}$ mice were transplanted with BALB/c skins. Adoptive transfer of $TCF1^{hi}CD4^+CD44^+$ but not $TCF1^-CD4^+CD44^+$ polyclonal T cells induced skin allograft rejection in *Rag1*$^{-/-}$ mice (Fig. 2c).

To obtain the alloantigen-specific $CD4^+$ T_{EP} cells, naive $CD45.1^+$ *Tcf7*^{GFP} TEa cells were adoptively transferred into $CD45.2^+$ WT B6 recipients 1 d before BALB/c heart transplantation. At 7 d post-heart transplantation, $TCF1^{hi}$ T_{EP} TEa and $TCF1^-$ effector TEa cells were isolated from the spleens and adoptively re-transferred into *Rag1*$^{-/-}$ mice. One day later, *Rag1*$^{-/-}$ mice were transplanted with BALB/c skins (Fig. 2d). Adoptive transfer of $TCF1^{hi}$ T_{EP} TEa but not $TCF1^-$ effector TEa cells induced skin transplant rejection (Fig. 2e). At 21 d post-skin transplantation, TEa cells were detected in the secondary lymphoid organs and enriched in the skin allografts in the $TCF1^{hi}$ T_{EP} TEa cell transfer group. By contrast, TEa cells were barely detectable in any examined tissues of *Rag1*$^{-/-}$ recipients that were transferred with $TCF1^-$ effector TEa cells (Fig. 2f,g).

We used a serial transplantation model to demonstrate the stemness of $TCF1^{hi}CD4^+$ T_{EP} cells. Naive $CD45.1^+$ *Tcf7*^{GFP} TEa cells were adoptively transferred into WT B6 mice (recipient 1) 1 d before BALB/c heart transplantation. At 7 d post-heart transplantation, $TCF1^{hi}$ T_{EP} TEa cells were isolated from heart transplant recipients and adoptively transferred into *Rag1*$^{-/-}$ mice (recipient 2) that were transplanted with BALB/c skins 1 d later. At 21 d post-skin transplantation, $TCF1^{hi}$ T_{EP} TEa and $TCF1^-$ effector TEa cells were isolated from those recipients and adoptively transferred into new *Rag1*$^{-/-}$ mice (recipient 3) that were transplanted with BALB/c skins 1 d later (Fig. 2h). Adoptive transfer of $TCF1^{hi}$ T_{EP} TEa cells from recipient 2 into recipient 3 drove skin transplant rejection, whereas $TCF1^-$ effector TEa cells failed to do so (Fig. 2i). Taken together, adoptive transfer of

TCF1^{hi} stem-like CD4^{+} T_{EP} cells but not TCF1^{-}CD4^{+} effector cells induces transplant rejection.

CD4^{+} T_{EP} cells are a source for effector T cells in alloimmunity

We further determined the distinct phenotypes and functions between CD4^{+} T_{EP} cells and effectors. *Rag1*$^{-/-}$ mice were adoptively transferred with naive CD45.1^{+} *Tcf7*^{GFP} TEa cells and transplanted with BALB/c skins (Extended Data Fig. 2c). Allografts were rejected 12–20 d post-transplantation (Extended Data Fig. 2d). In line with allograft rejection, TCF1^{+} TEa cells gradually developed into TCF1^{-} effectors, and virtually all graft-infiltrating TEa cells were TCF1^{-} (Extended Data Fig. 2e,f). TCF1^{hi} T_{EP} TEa and TCF1^{-} effector TEa cells were isolated from the secondary lymphoid organs at 14 d post-transplantation. Isolated TEa cells were either stimulated in vitro or adoptively transferred into new *Rag1*$^{-/-}$ mice 1 d before BALB/c skin transplantation. TCF1^{hi} T_{EP} TEa cells proliferated extensively in response to in vitro stimulation with T cell-depleted CB6F1 (F1 of Balb/c × B6) splenocytes (Fig. 3a). In contrast, TCF1^{-} effector TEa cells failed to proliferate and were instead prone to apoptosis. These effector cells expressed high levels of active caspase 3 and exhibited increased annexin V staining, which can be partially reversed by pan-caspase inhibition (Fig. 3a–c). Moreover, adoptive transfer of 1×10^4 TCF1^{hi} T_{EP} TEa cells drove skin graft rejection, whereas adoptive transfer of 100-fold more TCF1^{-} effector TEa cells could not induce transplant rejection (Fig. 3d). To understand these contrasting graft survival outcomes, transferred TEa cells were analyzed at 14 d post-transplantation. In recipients that had been transferred with 1×10^6 TCF1^{-} effector TEa cells, the transferred cells were notably absent in all examined tissues. In contrast, in recipients transferred with TCF1^{hi} T_{EP} TEa cells, the transferred cells migrated the allograft, intestine, colon and all examined secondary lymphoid tissues, exhibiting the ability to self-renew and to differentiate into TCF1^{-} effectors (Fig. 3e,f and Extended Data Fig. 2g).

Ly108 is a surrogate of TCF1 in stem-like precursors[4,38] and its gene expression inversely correlated to *Cxcr6* expression (Fig. 1c,d). Here we use Ly108^{hi}CXCR6^{-} and Ly108^{lo}CXCR6^{+} as cell surface markers for alloreactive CD4^{+} T_{EP} cells and effectors, respectively. In the above transplantation model (Extended Data Fig. 2c), Ly108^{hi}CXCR6^{-} T_{EP} TEa cells derived from the transferred naive *Tcf7*^{GFP} TEa cells expressed high or intermediate levels of TCF1^{GFP} (Fig. 3g), and they proliferated extensively in response to in vitro stimulation with CB6F1 splenocytes (Fig. 3h). Upon adoptive transfer into new *Rag1*$^{-/-}$ mice 1 d before BALB/c skin transplantation, Ly108^{hi}CXCR6^{-} T_{EP} TEa cells self-renewed, gave rise to Ly108^{lo}CXCR6^{+} effectors, and induced skin transplant rejection (Fig. 3i–k and Extended Data Fig. 3a–c). By contrast, Ly108^{lo}CXCR6^{+} effector TEa cells lost TCF1 expression, barely proliferated after in vitro stimulation, and failed to induce transplant rejection in vivo as they largely disappeared within 2 weeks post-transferring into new *Rag1*$^{-/-}$ hosts (Fig. 3g–j and Extended Data Fig. 3a,b). *Cxcr6*$^{-/-}$ mice had impaired ability to reject BALB/c hearts (Extended Data Fig. 3d,e), suggesting that CXCR6 was both a marker and a regulator of effector T cells.

We validated that CXCR6^{+} CD4^{+} effectors in the rejected human kidney allografts had significantly lost TCF1 expression, whereas CXCR6^{-}CD4^{+} T cells in both peripheral blood

mononuclear cells (PBMCs) and allografts retained TCF1 expression (Fig. 3l,m). Those $CXCR6^{-}CD4^{+}$ T cells were highly proliferative after in vitro activation. $CXCR6^{+}CD4^{+}$ effectors from the grafts lost proliferative capacity (Fig. 3n), akin to murine $CD4^{+}$ effectors. Taken together, $TCF1^{-}$ (also $Ly108^{lo}CXCR6^{+}$) $CD4^{+}$ effectors lose proliferative capacity. $TCF1^{hi}$ (also $Ly108^{hi}CXCR6^{-}$) $CD4^{+}$ T_{EP} cells must continuously replenish the effector cell pool to drive transplant rejection.

TCF1 and IRF4 govern distinct stem-like features

The above findings show that $CD4^{+}$ T_{EP} cells possess key stem-like features such as self-renewal and differentiation potential. As $CD4^{+}$ T_{EP} cells express high levels of TCF1, we studied whether TCF1 regulates their stem-like features. WT TEa and *Tcf7*$^{-/-}$ TEa cells were adoptively co-transferred into *Rag1*$^{-/-}$ mice 1 d before BALB/c skin transplantation (Extended Data Fig. 4a). Compared with WT TEa cells, *Tcf7*$^{-/-}$ TEa cells exhibited a significantly decreased cell frequency but remained capable of producing interferon (IFN)-γ (Extended Data Fig. 4b,c). Furthermore, $Ly108^{hi}CXCR6^{-}$ T_{EP} cell populations were dramatically reduced in *Tcf7*$^{-/-}$ TEa cells (Fig. 4a and Extended Data Fig. 4d). We next overexpressed TCF1 in TEa cells. TCF1 overexpression retained most TEa cells at the $Ly108^{hi}CXCR6^{-}$ T_{EP} cell state (Fig. 4b and Extended Data Fig. 4e). Therefore, TCF1 sustains the stem-like $CD4^{+}$ T_{EP} cells. Because *Tcf7*$^{-/-}$ TEa cells could develop into effectors (Fig. 4a and Extended Data Fig. 4c,d), they induced skin transplant rejection after adoptive transfer into *Rag1*$^{-/-}$ mice (Fig. 4c). Mice with T cell-specific TCF1 deletion (*Tcf7*$^{fl/fl}$*Cd4*-Cre) also promptly rejected BALB/c hearts (Extended Data Fig. 4f,g).

Next, we aimed to identify the molecular determinants that govern the effector differentiation potential of stem-like $CD4^{+}$ T_{EP} cells. We previously demonstrated that ablation of IRF4 in T cells induces transplant tolerance[29,35]. To determine whether IRF4 regulates the differentiation potential of $CD4^{+}$ T_{EP} cells, we tracked the adoptively co-transferred WT TEa and *Irf4*$^{-/-}$ TEa cells in *Rag1*$^{-/-}$ mice receiving BALB/c skins (Extended Data Fig. 5a). Frequencies of *Irf4*$^{-/-}$ TEa cells among the total transferred TEa cells in blood gradually decreased following transplantation (Extended Data Fig. 5b). At 14 d post-transplantation, virtually all *Irf4*$^{-/-}$ TEa cells in the secondary lymphoid organs retained the $Ly108^{hi}CXCR6^{-}$ (also $TCF1^{hi}$) T_{EP} cell state (Fig. 4d,e and Extended Data Fig. 5c,d). Therefore, *Irf4*$^{-/-}$$CD4^{+}$ T cells can develop into T_{EP} cells, but those T_{EP} cells lose effector differentiation potential. In line with this finding, *Irf4*$^{-/-}$ TEa cells did not infiltrate into allografts (Fig. 4f).

Trimethylation of H3K27 (H3K27me3) at the *Tcf7* locus is crucial for downregulating TCF1 during T cell effector differentiation[12]. We analyzed the transferred TEa cells at 14 d post-transplantation. Notably, in contrast to WT TEa cells, *Irf4*$^{-/-}$ TEa cells displayed minimal levels of H3K27me3 deposition at multiple regions of the *Tcf7* locus (Fig. 4g,h). This observation further underscores the inability of *Irf4*$^{-/-}$ TEa cells to downregulate TCF1. Moreover, compared to WT TEa cells, *Irf4*$^{-/-}$ TEa cells barely produced IFN-γ and granzyme B (Extended Data Fig. 5e,f). These data further indicate that in the absence of IRF4, alloreactive $CD4^{+}$ T cells are unable to differentiate into $TCF1^{-}$ effector cells.

We also adoptively transferred IRF4-transduced *Irf4*$^{-/-}$ TEa cells into *Rag1*$^{-/-}$ mice 1 d before BALB/c skin transplantation. IRF4 transduction restored the ability of *Irf4*$^{-/-}$ TEa cells to develop into TCF1^{-} (also CXCR6^{+}) effectors (Fig. 4i and Extended Data Fig. 5g) and infiltrate into allografts (Fig. 4j). While the adoptive transfer of *Irf4*$^{-/-}$ TEa cells failed to induce skin allograft rejection in *Rag1*$^{-/-}$ mice, transduction with IRF4 restored their ability to cause skin allograft rejection (Fig. 4k). Collectively, IRF4 governs the effector differentiation potential of CD4^{+} T_{EP} cells.

A previous study showed that T_H1 but not T_H2 cells express CXCR6 (ref. 41). To determine whether the T_H1 master regulator T-bet affects the generation of CXCR6^{+} CD4^{+} effectors, WT TEa and *Tbx21*$^{-/-}$ TEa cells were adoptively co-transferred into *Rag1*$^{-/-}$ mice receiving BALB/c skins. Deletion of T-bet did not abrogate the generation of Ly108^{hi}CXCR6^{-} T_{EP} cells and Ly108^{lo}CXCR6^{+} effectors (Extended Data Fig. 6a,b). Though the graft-infiltrating ability of *Tbx21*$^{-/-}$ TEa cells was impaired (Extended Data Fig. 6a), adoptive transfer of *Tbx21*$^{-/-}$ TEa cells alone induced skin allograft rejection in *Rag1*$^{-/-}$ recipients (Extended Data Fig. 6c,d). Thus, T-bet is dispensable for the generation of Ly108^{lo}CXCR6^{+} effectors. Taken together, TCF1 sustains CD4^{+} T_{EP} cells, whereas IRF4 governs their effector differentiation potential.

scRNA-seq identifies LDHA as a regulator of CD4^{+} T cell alloimmunity

After activation, T cells undergo extensive metabolic rewiring to meet the demand of vigorous cell proliferation[19,20]. Both CD4^{+} T_{EP} cells and effectors are activated T cells, but the metabolic profiles reflecting their cell states remain unknown. Here we applied a Compass algorithm to quantitatively profile the metabolic state of every TEa cell in the scRNA-seq data (related to Fig. 1)[26]. The Compass identified 1,497 reactions in 79 metabolic subsystems that were significantly differentially active between stem-like T_{EP} (clusters 0 and 2) and effector (cluster 1) TEa cells. Most of those reactions were more active in effectors than in stem-like T_{EP} cells, as shown in all 79 subsystems (Extended Data Fig. 7a) and illustrated in more detail in eight subsystems (such as glycolysis; Fig. 5a–c and Extended Data Fig. 7b). Many reactions were positively correlated with the expression of effector genes *Cxcr6*, *Nkg7*, *Tnfrsf4*, *Tnfrsf18* and *Gzmb* (Extended Data Fig. 7c).

Glycolysis stood out as one of the most significant subsystems with active reactions in effectors (Fig. 5a and Extended Data Figs. 7a and 8a). Thus, we analyzed the expression of genes encoding critical enzymes that catalyze sequential reactions in glycolysis. Compared to T_{EP} TEa cells, effector TEa cells exhibited elevated expression of *Gpi1*, *Aldoa*, *Tpi1*, *Gapdh*, *Pgk1*, *Pgam1*, *Eno1*, *Pkm* and *Ldha* (Extended Data Fig. 8b,c).

LDHA catalyzes the final step of glycolysis by converting pyruvate to lactate (Extended Data Fig. 8b)[21]. To determine the role of LDHA in allogeneic T cell response, we generated the *Ldha*$^{fl/fl}$*Cd4*-Cre mice to delete LDHA in T cells. *Ldha*$^{-/-}$ TEa mice were then generated by crossing *Ldha*$^{fl/fl}$*Cd4*-Cre with CD45.1^{+} TEa mice. Next, we adoptively transferred *Ldha*$^{-/-}$ TEa cells into B6 mice 1 d before BALB/c heart transplantation. As *Ldha*$^{-/-}$ TEa cells did not infiltrate into allografts, we isolated *Ldha*$^{-/-}$ TEa cells from spleens at 7 d post-transplantation for scRNA-seq analysis. scRNA-seq data of WT TEa cells in the spleens of heart transplant recipients were used for comparison. Clustering analysis identified eight

clusters of cells from both *Ldha*$^{-/-}$ TEa and WT TEa cells (Extended Data Fig. 9a,b). WT TEa cells in clusters 6 and 7 displayed effector-like cell state, expressing key effector genes *Cxcr6*, *Gzmb*, *Ifng* and *Nkg7*. In contrast, *Ldha*$^{-/-}$ TEa cells largely failed to express these key effector genes in response to heart transplantation (Fig. 5d).

TEa cell clusters 0 to 4 expressed high levels of *Tcf7*, *Sell* and *Ccr7*, indicative of a stem-like cell state (Fig. 5d,e). We applied the Compass algorithm to profile the metabolic state of stem-like TEa cell populations. Indeed, the majority of glycolytic reactions were less active in *Ldha*$^{-/-}$ stem-like TEa cells than in WT stem-like TEa cells, particularly in the case of L-lactate dehydrogenase reaction (Fig. 5f). Reactions in several other metabolic subsystems, such as the citric acid cycle, oxidative phosphorylation and glutamate metabolism, were generally more active in *Ldha*$^{-/-}$ stem-like TEa cells than in WT stem-like TEa cells (Extended Data Fig. 9c,d). Taken together, scRNA-seq analysis identifies LDHA as a crucial regulator for stem-like T_{EP} cells to differentiate into effector cells.

LDHA controls effector differentiation potential

Ldha was highly expressed in effector TEa cells (Extended Data Fig. 10a). To further elucidate the role of LDHA in the allogeneic T cell response, *Ldha*$^{fl/fl}$*Cd4*-Cre and *Ldha*$^{fl/fl}$ control mice were transplanted with BALB/c hearts (Extended Data Fig. 10b). All *Ldha*$^{fl/fl}$*Cd4*-Cre recipients accepted BALB/c heart allografts in the absence of any immunosuppressive treatments, whereas *Ldha*$^{fl/fl}$ control mice acutely rejected their heart allografts (Fig. 6a). To determine the role of LDHA in alloantigen-specific CD4$^+$ T cells, *Ldha*$^{-/-}$ TEa and WT TEa cells were adoptively transferred into *Rag1*$^{-/-}$ mice 1 d before BALB/c skin transplantation (Extended Data Fig. 10c). Adoptive transfer of WT TEa cells induced skin allograft rejection, but *Ldha*$^{-/-}$ TEa cells failed to do so (Fig. 6b). Hence, LDHA is required for CD4$^+$ T cell alloimmunity.

To understand why *Ldha*$^{-/-}$CD4$^+$ T cells cannot induce transplant rejection, CellTrace Violet (CTV)-labeled WT TEa and *Ldha*$^{-/-}$ TEa cells were adoptively co-transferred into *Rag1*$^{-/-}$ mice 1 d before BALB/c skin transplantation (Extended Data Fig. 10d), followed by flow cytometric analysis at 14 d post-transplantation. WT TEa but not *Ldha*$^{-/-}$ TEa cells infiltrated into skin allografts (Extended Data Fig. 10e). In the secondary lymphoid organs, both WT TEa and *Ldha*$^{-/-}$ TEa cells proliferated extensively based on the CTV dilution. Highly proliferated CTV$^-$ but not less-proliferated CTV$^+$ WT TEa cells developed into effectors, characterized by the loss of TCF1 and Ly108 expression as well as the gain of CXCR6, IFN-γ and T-bet expression. *Ldha*$^{-/-}$ TEa cells were largely retained in the T_{EP} cell state, evident by their failure to develop into CTV$^-$TCF1$^-$, CTV$^-$Ly108$^-$ and CTV$^-$CXCR6$^+$ effectors (Fig. 6c and Extended Data Fig. 10f–h). Collectively, LDHA governs the effector differentiation potential of CD4$^+$ T_{EP} cells.

To investigate whether the deletion of LDHA affects the survival of alloreactive CD4$^+$ T cells during cell division, we further examined the transferred TEa cells for the expression of BCL2 and active caspase 3 on day 14 post-transplantation. In both WT and *Ldha*$^{-/-}$ TEa cell populations, the BCL2 expression level was higher in less-proliferated CTV$^+$ cells than in highly proliferated CTV$^-$ cells and active caspase 3$^+$ cells were detectable among CTV$^-$ cells but not among CTV$^+$ cells (Fig. 6d,e,g). Compared to WT TEa cells, *Ldha*$^{-/-}$

TEa cells displayed a higher level of BCL2 expression in the CTV^- cell population and had fewer CTV^- active caspase 3^+ cells (Fig. 6d,f,g). Through this analysis, we did not detect an increase in apoptosis in *Ldha*$^{-/-}$ TEa cells compared to WT TEa cells. Taken together, LDHA is essential for alloreactive $CD4^+$ T_{EP} cells to differentiate into $CXCR6^+$ effector cells and the deletion of LDHA in T cells alone induces transplant acceptance.

Discussion

In this study, we used scRNA-seq to analyze transcriptomic changes in alloantigen-specific $CD4^+$ T cells following heart transplantation. This analysis led to the identification of two major alloreactive $CD4^+$ T cell populations: $TCF1^+Ly108^+$ T_{EP} cells and $TCF1^-CXCR6^+$ effectors. T_{EP} cells displayed stem-like features, including self-renewal and the potential for further effector differentiation. Effector cells, however, lost their proliferative ability, became prone to apoptosis and did not persist. Thus, the continuous replenishment of effector cells from the stem-like T_{EP} cells is crucial in driving transplant rejection.

We provide evidence that within the $CD4^+$ T_{EP} cell compartment, the capacity for self-renewal and the potential for effector differentiation are regulated by distinct mechanisms. Akin to the role of TCF1 in stem-like $CD8^+$ T cells[9–11], TCF1 is a crucial regulator for the self-renewal of $CD4^+$ T_{EP} cells. The deletion of TCF1 significantly decreased T_{EP} cell frequency in transplant recipients. On the other hand, $CD4^+$ T_{EP} cells relied on IRF4 and LDHA for further effector differentiation. In the absence of either IRF4 or LDHA, T_{EP} cells were unable to differentiate into $TCF1^-CXCR6^+$ effectors, resulting in transplant acceptance. The specific functions of $TCF1^-CXCR6^+$ effectors, however, remain an open question. These effectors were the primary population of $CD4^+$ T cells in the allograft. They expressed high levels of key effector genes that encode CXCR6 (refs. 4,39), T-bet, granzyme B, IFN-γ, GITR, OX40 and NKG7 (ref. 40). Notably, without T-bet, $CD4^+$ T_{EP} cells could still differentiate into $CXCR6^+$ effectors, thereby leading to transplant rejection. Conversely, *Cxcr6* deficiency significantly prolonged heart allograft survival. Further investigation into this effector cell population will expand our understanding of $CD4^+$ T cell-mediated tissue destruction.

IRF4 controls the differentiation of several T_H cell subsets and binds directly to specific cytokine gene loci, including *Il4*, *Il9*, *Il17a* and *Il21* (refs. 14–18,42,43). In our research, we found that without IRF4, alloreactive $CD4^+$ T cells could not downregulate TCF1 expression. This effect seems related to H3K27me3 deposition at the *Tcf7* locus, a key mechanism for silencing TCF1 during T cell effector differentiation[12]. The deletion of IRF4 prevented H3K27me3 deposition at various regions of the *Tcf7* locus in alloreactive $CD4^+$ T cells. Moreover, the deletion of IRF4 also inhibited the expression of CXCR6, IFN-γ, and granzyme B in alloreactive $CD4^+$ T cells. These data collectively indicate that in the absence of IRF4, alloreactive $CD4^+$ T_{EP} cells are unable to differentiate into $TCF1^-CXCR6^+$ effector cells.

Proinflammatory T_H17 cells play a pivotal pathogenic role in autoimmunity[4,44]; however, in the absence of specific stimuli such as IL-1β and IL-23, they exhibit a non-pathogenic state[45]. In a landmark study, Wagner et al. developed the Compass algorithm to dissect

the metabolic profiles of both non-pathogenic and pathogenic T_H17 cells[26]. Using this algorithm, in conjunction with multiple metabolic assays, the authors discovered that pathogenic T_H17 cells display an elevated level of aerobic glycolysis. In contrast, non-pathogenic T_H17 cells, mirroring regulatory T cells, preferentially utilize fatty acid oxidation to generate ATP. We applied the Compass algorithm[26] to analyze the metabolic profiles of alloreactive $CD4^+$ T cells. In line with pathogenic T_H17 cells, alloreactive $CD4^+$ effector T cells also exhibited an elevated level of glycolysis. To investigate this further, we deleted LDHA in T cells. Without LDHA, the majority of glycolytic reactions became less active in *Ldha*$^{-/-}$ stem-like T_{EP} cells than in WT stem-like T_{EP} cells, particularly in the case of the L-lactate dehydrogenase reaction. Notably, in the absence of LDHA, stem-like $CD4^+$ T_{EP} cells were unable to differentiate into $TCF1^-CXCR6^+$ effector cells.

While $TCF1^-$ effector T cells were crucial for mediating transplant rejection, they lost their proliferative capability, became prone to apoptosis and lacked persistence. Therefore, adoptively transferring these effector cells alone into secondary hosts was insufficient to induce transplant rejection. In contrast, $TCF1^+CD4^+$ T_{EP} cells displayed dual features of self-renewal and the potential for effector differentiation. Allograft rejection relied on the continuous replenishment of the effector T cell pool from these stem-like T_{EP} cells. Moreover, in line with Schnell et al.'s findings in autoimmunity[4], our research identifies Ly108 and CXCR6 as valuable surface markers for distinguishing between stem-like and effector $CD4^+$ T cell populations in transplantation, underlining a striking parallel between autoimmunity and transplantation contexts.

In summary, $CD4^+$ T_{EP} cells serve as a continuous source for the generation of effector cells. Targeting these stem-like $CD4^+$ T_{EP} cells could be a new strategy for eliminating allogeneic or other deleterious T cell responses.

Online content

Any methods, additional references, Nature Portfolio reporting summaries, source data, extended data, supplementary information, acknowledgements, peer review information; details of author contributions and competing interests; and statements of data and code availability are available at https://doi.org/10.1038/s41590-023-01682-z.

Methods

Mice

C57BL/6 (WT B6, $CD45.2^+$), B6.SJL-*Ptprc*^{a} *Pepc*^{b}/*Boy*J (B6, $CD45.1^+$), B6.Cg-Tg(Tcra,Tcrb)3Ayr/J (TEa TCR transgenic), B6(Cg)-*Tcf7*^{tm1Hhx}/J (*Tcf7*^{GFP} flox; referred to as *Tcf7*^{GFP}), B6.129S1-*Irf4*^{tm1Rdf}/J (*Irf4*^{fl}), B6(Cg)-*Ldha*$^{tm1c(EUCOMM)Wtsi}$/DatsJ (*Ldha*^{fl}), Tg(Cd4-cre)1Cwi/BfluJ (*Cd4*-Cre), B6.129S7-*Rag1*^{tm1Mom}/J (*Rag1*$^{-/-}$), C.129P2-*Cxcr6*^{tm1Litt}/J (*Cxcr6*$^{-/-}$) and C.129S6-*Tbx21*^{tm1Glm}/J (*Tbx21*$^{-/-}$) mice are all on a C57BL/6 background. The above mouse strains and BALB/c mice were purchased from the Jackson Laboratory. Female BABL/c and male B6 mice were crossed to generate CB6F1 mice. CD45.1 and TEa mice were crossed to generate $CD45.1^+$ TEa mice. *Tcf7*^{GFP} flox and $CD45.1^+$ TEa mice were crossed to generate $CD45.1^+$ *Tcf7*^{GFP} TEa mice. *Cd4*-Cre and

Tcf7^{GFP} flox mice were crossed to generate *Tcf7*$^{fl/fl}$*Cd4*-Cre mice. *Tcf7*$^{fl/fl}$*Cd4*-Cre and CD45.1$^+$ TEa mice were crossed to generate *Tcf7*$^{fl/fl}$*Cd4*-Cre CD45.1$^+$ TEa (referred to as CD45.1$^+$ *Tcf7*$^{-/-}$ TEa) mice. *Cd4*-Cre and *Irf4*^{fl} mice were crossed to generate *Irf4*$^{fl/fl}$*Cd4*-Cre mice. *Irf4*$^{fl/fl}$*Cd4*-Cre were crossed with TEa mice to generate *Irf4*$^{fl/fl}$*Cd4*-Cre TEa (referred to as *Irf4*$^{-/-}$ TEa) mice. *Cd4*-Cre and *Ldha*^{fl} mice were crossed to generate *Ldha*$^{fl/fl}$*Cd4*-Cre mice. *Ldha*$^{fl/fl}$*Cd4*-Cre were crossed with TEa mice to generate *Ldha*$^{fl/fl}$ *Cd4*-Cre TEa (referred to as *Ldha*$^{-/-}$ TEa) mice. *Tbx21*$^{-/-}$ mice were crossed with CD45.1$^+$ TEa mice to generate CD45.1$^+$ *Tbx21*$^{-/-}$ TEa mice. All mice were bred and maintained in specific-pathogen-free conditions at Houston Methodist Hospital. All mice were housed with access to water and a standard laboratory diet and were maintained on a 12-h light–dark cycle at temperatures of 68–79 °F and humidity levels between 30–70%. Mice at 8–12 weeks old (both sexes) were used for all experiments. Age- and sex-matched mice were randomized and used for experiments. All animal experiments in this study were approved by the Houston Methodist Animal Care Committee in accordance with institutional animal care and use guidelines.

Mouse heart and skin transplantation

Heart and skin transplantation were performed as previously described[29,36]. For heart transplantation, the donor heart aorta and pulmonary artery were anastomosed to the recipient abdominal aorta and inferior vena cava, respectively. Heart graft survival was monitored daily by palpation. Complete cessation of heartbeat was considered as graft rejection. For skin transplantation, ~1.0 × 1.0 cm donor tail skins were transplanted onto the backs of recipients. More than 90% necrosis of the donor skin tissue was considered graft rejection.

Adoptive transfer of polyclonal CD4$^+$ T cells

Tcf7^{GFP} mice were transplanted with BALB/c hearts. Ten thousand TCF1^{hi} or TCF1^{lo} cells were sorted from CD4$^+$CD44$^+$ splenocytes at 7 d after heart transplantation, and adoptively transferred into *Rag1*$^{-/-}$ recipients that were transplanted with BALB/c skins 1 d later.

Adoptive transfer of WT TEa and genetically modified TEa cells

The TCR transgenic TEa CD4$^+$ T cells recognize a major histocompatibility complex class II I-Eα alloantigen presented by I-A^b. Naive TEa cells were isolated from WT TEa and genetically modified TEa mice using Dynabeads untouched mouse CD4 cells kit (Thermo Fisher Scientific). In the heart transplantation model, CD45.2$^+$ WT B6 mice were adoptively transferred with 1 × 10^6 CD45.1$^+$ naive TEa cells 1 d before BALB/c heart transplantation. The transferred TEa cells were obtained from spleens and allografts at 7 d post-transplantation for scRNA-seq and flow cytometric analyses. In the skin transplantation models, *Rag1*$^{-/-}$ mice were adoptively transferred with 1 × 10^5 naive WT, *Tcf7*$^{-/-}$, *Irf4*$^{-/-}$, IRF4-transduced *Irf4*$^{-/-}$, *Tbx21*$^{-/-}$ or *Ldha*$^{-/-}$ TEa cells, followed by BALB/c skin transplantation 1 d later. In the adoptive co-transfer models, *Rag1*$^{-/-}$ mice were transferred with 1 × 10^5 WT TEa cells together with 1 × 10^5 genetically modified TEa cells (congenically marked *Tbx21*$^{-/-}$, *Tcf7*$^{-/-}$, *Irf4*$^{-/-}$ or *Ldha*$^{-/-}$ TEa cells, respectively). *Rag1*$^{-/-}$ mice were then transplanted with BALB/c skins 1 d later.

Adoptive transfer of T_{EP} TEa and effector TEa cells

CD45.2$^+$ WT B6 mice were adoptively transferred with 1 × 10^6 naive CD45.1$^+$ *Tcf7*^{GFP} TEa cells, followed by BALB/c heart transplantation on the next day. On day 7 post-heart transplantation, 1 × 10^4 TCF1^{hi} or TCF1$^-$ TEa cells were sorted from the secondary lymphoid organs and re-transferred into *Rag1*$^{-/-}$ hosts, followed by BALB/c skin transplantation the next day.

In another model, *Rag1*$^{-/-}$ mice were adoptively transferred with 1 × 10^6 naive CD45.1$^+$ *Tcf7*^{GFP} TEa cells, followed by BALB/c skin transplantation 1 d later. On day 14 post-skin transplantation, various numbers of TCF1^{hi} or TCF1$^-$ TEa cells (or 1 × 10^5 Ly108^{hi}CXCR6$^-$ or Ly108^{lo}CXCR6$^+$ TEa cells) were sorted from the secondary lymphoid organs and re-transferred into *Rag1*$^{-/-}$ hosts, followed by BALB/c skin transplantation the next day.

Serial transplantation

Serial transplantation models are often used to demonstrate the T cell stemness[38,46]. Here CD45.2$^+$ WT B6 mice (recipient 1) were adoptively transferred with 1 × 10^6 naive CD45.1$^+$ *Tcf7*^{GFP} TEa cells and transplanted with BALB/c hearts. At 7 d post-heart transplantation, 1 × 10^5 TCF1^{hi} TEa cells were sorted from the secondary lymphoid organs and were re-transferred into *Rag1*$^{-/-}$ hosts (recipient 2) that were transplanted with BALB/c skins. At 21 d post-skin transplantation, 1 × 10^4 TCF1^{hi} or TCF1$^-$ TEa cells were isolated from recipient 2 and were re-transferred into new *Rag1*$^{-/-}$ mice (recipient 3) that were transplanted with BALB/c skins.

Preparation of single-cell suspension

Lymph nodes and spleens were mechanically disrupted with the back of a 1-ml syringe, filtered through a 70-μm cell strainer, and incubated with ACK lysis buffer (Thermo Fisher Scientific) to remove red blood cells. Cells were washed twice with cold PBS supplemented with 2% fetal bovine serum (FBS).

To obtain graft-infiltrating cells, heart and skin allografts were minced into small pieces and incubated with 450 U ml^{-1} collagenase I (Thermo Fisher Scientific) and 60 U ml^{-1} DNase I (Thermo Fisher Scientific) solution in a shaker at 37 °C for 45 min. After digestion, the tissues were mechanically disrupted with the back of a 1-ml syringe, filtered through a 70-μm cell strainer and washed twice with cold PBS supplemented with 10% FBS, as modified from a previously described protocol[47]. Leukocytes from the obtained cell suspensions were then purified through Percoll gradient centrifugation (GE Healthcare), followed by removing red blood cells with ACK lysis buffer.

Cells were isolated from the intestine and colon using a method previously described[4]. To remove epithelial cells and intraepithelial lymphocytes, tissues from the intestine and colon of transplant recipients were cleaned and then incubated with RPMI 1640 medium (Thermo Fisher Scientific), supplemented with 5% FBS, 1 mM dithiothreitol (Thermo Fisher Scientific) and 5 mM EDTA (Thermo Fisher Scientific). This incubation was carried out at 37 °C for 20 min, with continuous stirring at 350 r.p.m. Subsequently, for tissue

digestion, pretreated tissues were minced into smaller pieces and then incubated with RPMI 1640 medium, supplemented with 5% FBS, 50 μg ml^{-1} DNase I (Sigma-Aldrich), 1 mg ml^{-1} Collagenase Type VIII (Sigma-Aldrich), 2 mM $CaCl_2$ (Sigma-Aldrich) and 5 mM $MgCl_2$ (Sigma-Aldrich). This incubation was conducted at 37 °C for 40 min, with continuous stirring at 550 r.p.m. After digestion, the tissues were passed through 40-μm sterile strainers to isolate the cells.

Flow cytometric analysis and cell sorting

Antibodies were purchased from BioLegend, Thermo Fisher Scientific, BD Biosciences and Cell Signaling Technology. For cell surface staining, single-cell suspensions were incubated with a Zombie Aqua Fixable Viability kit (BioLegend) for 15 min and then incubated with fluorochrome-conjugated antibodies for 15 min in the dark at 4 °C. The following antibodies were used for mouse cell surface staining: CD45 (1:200 dilution, Clone 30-F11), CD45.1 (1:200 dilution, A20), CD45.2 (1:200 dilution, 104), CD4 (1:200 dilution, GK1.5), TCR Vα2 (1:200 dilution, B20.1), TCR Vβ6 (1:200 dilution, RR4–7), Ly108 (1:200 dilution, 330-AJ), GITR (1:200 dilution, DTA-1), CXCR6 (1:200 dilution, SA051D1) and CD44 (1:200 dilution, IM7). The following antibodies were used for human cell surface staining: CD4 (1:100 dilution, RPA-T4), CXCR6 (1:100 dilution, K041E5) and CD45 (1:100 dilution, HI30). For intracellular staining of transcription factors TCF1 (1:100 dilution, Clone S33–966 or C63D9), BCL2 (1:100 dilution, 10C4) and T-bet (1:100 dilution, 4B10), the FOXP3/Transcription Factor Staining Buffer Set (Thermo Fisher Scientific) was used according to manufacturer's instructions. For intracellular cytokine staining, cells were stimulated for 5 h with 50 ng ml^{-1} phorbol 12-myristate 13-acetate and 500 ng ml^{-1} ionomycin (Sigma-Aldrich) in the presence of GolgiStop (BD Biosciences), fixed and permeabilized with Cytofix/Cytoperm solution (BD Biosciences) or using the FOXP3/Transcription Factor Staining Buffer Set and stained with antibody specific for mouse IFN-γ (1:200 dilution, XMG1.2) and granzyme B (1:200 dilution, QA16A02), as previously described[29]. For intracellular staining of active caspase 3, cells were fixed and permeabilized using Cytofix/Cytoperm solution (BD Biosciences), then stained with an antibody specific for active caspase 3 (1:100 dilution, Clone C92–605; BD Biosciences). The staining of annexin V (cat. 640947; BioLegend) was performed according to manufacturer's instructions. Cells were analyzed by an LSRII & Fortessa flow cytometer with BD FACS Diva software (v.8.0.2) (BD Biosciences) or sorted by an FACSAria cell sorter (BD Biosciences). Flow cytometric data were analyzed with FlowJo v.10 software (Tree Star).

In vitro proliferation of T_{EP} TEa and effector TEa cells

To obtain T cell-depleted stimulators, B6 and CB6F1 splenocytes were incubated with anti-mouse CD3 (clone 17A2) for 15 min, followed by incubation with the Depletion Dynabeads (Thermo Fisher Scientific). To obtain responder cells, the adoptively transferred $TCF1^{hi}$, $TCF1^{-}$, $Ly108^{hi}CXCR6^{-}$ and $Ly108^{lo}CXCR6^{+}$ TEa cells were sorted from the secondary lymphoid organs of transplant recipients. Naive TEa cells were used as control responder cells. Sorted TEa cells were labeled with CTV (Thermo Fisher Scientific) following the manufacturer's protocol. CTV-labeled TEa cells (1×10^5 per well) were co-cultured with B6 or CB6F1 stimulators (2×10^5 per well) in 96-well plates in the presence of 10 U ml^{-1}

rIL-2 (PeproTech) at 37 °C, 5% CO_2, followed by flow cytometric analysis on day 3 after stimulation.

In vitro cell apoptosis assay

TCF1^{hi} and TCF1^{-} TEa cells were sorted from the secondary lymphoid organs of transplant recipients. These cells (1×10^5 per well) were co-cultured with T cell-depleted CB6F1 splenocytes (2×10^5 per well) in 96-well plates, in the presence of 10 U ml^{-1} rIL-2 at 37 °C, 5% CO_2 for 3 d. To determine the effects of pan-caspase inhibition on effector TEa cells, TCF1^{-} TEa cells were treated with or without 30 μM Z-VAD-FMK (Selleckchem) for 3 d. Subsequently, active caspase 3 expression and annexin V staining of TEa cells were analyzed using a Fortessa flow cytometer.

Chromatin immunoprecipitation

ChIP assays were performed using a ChIP-IT PBMC Kit (Active Motif) according to manufacturer's instructions. In brief, WT TEa or *Irf4*$^{-/-}$ TEa cells were adoptively transferred into *Rag1*$^{-/-}$ recipients 1 d before BALB/c skin transplantation. These transferred TEa cells were sorted from the secondary lymphoid tissues of the recipients 14 d post-transplantation. Next, 2×10^6 sorted cells per sample were fixed with formaldehyde and subjected to sonication using a QSonica800R3 at 85% amplitude for a total sonication duration of 1 h. Immunoprecipitation of chromatin was performed using anti-histone H3K27me3 (cat. 39155; Active Motif) and an isotype-matched control antibody (sc-2027; Santa Cruz). Then, 5 μg of antibodies was used for each ChIP. Subsequently, the precipitated DNA was analyzed by real-time PCR. The results were presented as relative binding, normalized to input DNA. The primers used in ChIP–qPCR were purchased from Integrated DNA Technologies (IDT). *Tcf7* Promoter: forward CCTTCGGACTCATTCACCAG; reverse GCGAGGAACAGGACGATAAG. *Tcf7* 5′ UTR: forward CGGTGCCCTGACCTTTAT; reverse: CTCCGAACGGGTGGAAATA; *Tcf7* CNS: forward CCATGCTAGAAGGATGATCAGG; reverse GCCCAGAAAGAAGAGGTAACA *Tcf7* 3′ UTR: forward GGCTCTTCCCAGTTCCATTT; reverse AGGCTCAGGGTTAAGTTTGG.

Retrovirus-mediated gene expression

For IRF4 overexpression, retroviral particles were produced by transfecting plat-E cells with the IRF4–GFP or empty control (Ctrl)–GFP retroviral vector (pMYs–IRES–eGFP, Cell Biolabs), as previously described[29]. Naive *Irf4*$^{-/-}$ TEa cells were stimulated with T cell-depleted CB6F1 splenocytes for 24 h, incubated with freshly prepared retroviral particles by centrifugation for 2 h at 780*g* and 32 °C in the presence of 8 μg ml^{-1} polybrene (Sigma-Aldrich) and cultured for 4 h at 32 °C. The transduced TEa cells were further cultured for 72 h in complete RPMI 1640 medium at 37 °C before cell sorting. Then, 100,000 sorted *Irf4*$^{-/-}$ TEa cells expressing IRF4–GFP or Ctrl–GFP were adoptively transferred into *Rag1*$^{-/-}$ mice 1 d before BALB/c skin transplantation.

For TCF1 overexpression, a pMYs–IRES-mCherry retroviral vector was generated by replacing eGFP in the pMYs–IRES–eGFP vector with mCherry. Mouse *Tcf7* cDNA (ORIGENE) was cloned into the pMYs–IRES–mCherry vector. Retroviral particles were produced by transfecting plat-E cells with the TCF1-mCherry or empty pMYs–IRES–

mCherry control (Ctrl-mCherry) vector. WT TEa cells were activated for 1 d with T cell-depleted CB6F1 splenocytes and transduced with freshly prepared retroviral particles as mentioned above. The transduced TEa cells were further cultured for 72 h before cell sorting. Then, 100,000 sorted mCherry^{+} TEa cells were adoptively transferred into *Rag1*$^{-/-}$ mice 1 d before BALB/c skin transplantation.

ScRNA-seq analysis of TEa cells

scRNA-seq was performed by the Single-Cell Genomics Core at Baylor College of Medicine. Single-cell Gene Expression Library was prepared according to Chromium Next GEM Single Cell 3′ Reagent kits v3 (10x Genomics). In brief, a single-cell suspension, reverse transcription reagents, gel beads containing barcoded oligonucleotides and oil were loaded onto a Chromium controller (10x Genomics) to generate single-cell GEMs (gel beads in emulsion) where full length cDNA was synthesized and barcoded for each single cell. Subsequently the GEMs were broken and complementary DNA from each single cell was pooled. Following cleanup using Dynabeads MyOne Silane Beads, cDNA was amplified by PCR. The amplified product was fragmented to the optimal size before end-repair, A-tailing and adaptor ligation. The final library was generated by amplification. After quantification with a KAPA Library Quantification kit (Roche), libraries were sequenced using a Novaseq 6000 (Illumina).

Raw Illumina sequencing reads were aligned to the reference mouse genome mm10 (Ensembl 93) using CellRanger v.7.0.0 with default parameters, generating one Fastq dataset for WT TEa cells from heart allografts, one for WT TEa cells from the spleens of transplant recipients and one for *Ldha*$^{-/-}$ TEa cells from the spleens of transplant recipients. For each of the three datasets, genes were quantified as unique molecular identifier counts using CellRanger count and initially visualized using Loupe Browser v.5.0.0.

Downstream analysis of the datasets from graft-infiltrating WT TEa and splenic WT TEa cells was performed using Seurat v.4.0.0 on filtered feature counts generated by CellRanger count. Low-quality single cells containing >2.5% mitochondrial transcripts or >50% ribosomal transcripts were removed. Additionally, genes expressed in fewer than three single cells were removed. We identified potential single-cell doublets using DoubletFinder v.2.0.3, with an expectation of a 7.5% doublet rate assuming Poisson statistics, as per the developer's code on GitHub. Following the removal of low quality and doublet cells, the graft-infiltrating WT TEa and splenic WT TEa datasets were combined in Seurat, and single-cell gene expression counts for 14,254 genes were normalized to the library size and $\log_2$-transformed in Seurat and batch-corrected using Harmony v.1.0. Normalized data for all available genes were scaled in Seurat and principal-component analyses were applied to reduce the dimensionality of the data using the top 2,000 most variable genes in the dataset. We used principal components as input for Louvain based graphing and chose resolution parameters of 0.8 to define eight clusters among 10,964 TEa cells, where 4,028 of 10,964 TEa cells were from heart allografts. Wilcoxon rank-sum tests were applied through the FindMarkers function in Seurat with logfc. threshold = 0.25 and min.pct = 0.05 to identify genes differentially expressed in each cluster versus all others as marker genes for each cluster. Feature plots and violin plots were generated via Seurat for key

marker genes to visualize the pattern of expressions across the whole dataset. The genes specifically expressed in each cluster were examined to define the name of the clusters, and additional Wilcoxon rank-sum tests were applied to identify genes with significant differential expressions between WT stem-like T_{EP} TEa cells (cluster 0 and 2) and WT effector TEa cells (cluster 1). A heat map summarizing the expression of 38 genes across eight clusters was generated using R package DoMultiBarHeatmap designed specifically for Seurat data objects.

The splenic WT TEa dataset and the splenic *Ldha*$^{-/-}$ TEa dataset were combined in Seurat and single-cell gene expression counts for 19,916 genes were normalized to the library size and $\log_2$-transformed in Seurat and batch-corrected using following the scRNA-seq integration pipeline defined by Stuart et al.[48] and applied through Seurat v.4.3.0. Normalized data for all available genes were scaled in Seurat and principal-component analyses were applied to reduce the dimensionality of the data using the top 2,000 most variable genes in the dataset. We used principal components as input for Louvain based graphing and chose resolution parameters of 0.3 to define eight clusters among 18,881 TEa cells. Wilcoxon rank-sum tests were applied through FindMarkers function in Seurat with logfc.threshold = 0.25 and min.pct = 0.05 to identify genes differentially expressed in each cluster versus all others as marker genes for each cluster. Feature plots and violin plots were generated via Seurat for key marker genes to visualize the pattern of expressions across the whole dataset. Specifically, for violin plots in Fig. 5d, the distribution of expression levels for each gene were summarized in each of the eight clusters and the subplot representing each cluster was further split into two halves based on the genetic background of TEa cells, with the *Ldha*$^{-/-}$ TEa cell population on the left in red and WT TEa cell population on the right in green.

GSEA for canonical pathways changed in each cluster

For the comparison of each cluster versus all other clusters, the FindMarkers function in Seurat was run with logfc.threshold = min.pct = 0 and min.cells.group = min.cells,feature = 1, thus generating P values from Wilcoxon rank-sum tests as well as $\log_2$ fold changes for all 14,254 genes detected in the dataset. For each cluster $X \in [0,7]$, gene set enrichment analysis (GSEA) was run on the pre-ranked list using the vector of $\log_2$ fold change from X versus all others for each gene to identify canonical pathways with significant enrichment of up- or downregulated genes in cluster X. The analysis was carried out using GSEAPreranked function in Broad Institute GSEA v.4.3.2 software. A total of 1,687 mouse specific canonical pathways from REACTOME, WIKIPATHWAYS and BioCarta database were tested for enrichment, with the list of member genes obtained from m2.cp.v2022.1.Mm.symbols.gmt in Molecular Signature Database v.Msigdb_v2022.1.Mm. We identified 801 pathways that were differentially expressed in WT TEa cell clusters. The enrichment results for 48 pathways across eight clusters were summarized in a bubble plot following the format defined in Bubble Gum (GSEA Unlimited Map) software. Because Bubble Gum does not currently support GSEAPreranked, the plot was generated from an in-house script using MATLAB.

Compass analysis of metabolic states in WT T_{EP} and effector cells

We applied the Compass algorithm and tool with default parameters for metabolic flux modeling using scRNA-seq dataset[26]. Each of the 10,964 WT TEa cells in our dataset was evaluated for the activities of 10,211 metabolic reactions from 99 metabolic subsystems defined in the Recon2 model. The Compass tool ran on a MacPro workstation with 4.4 GHz 12-core intel Xeon W processor and 96GB DDR4 ECC memory, and the average time for evaluating one cell was 63.22 s.

The clusters of WT TEa cells were illustrated in Fig. 1b. The Compass tool produced a 10,211 (reactions) × 10,964 (TEa cells) matrix recording reaction penalty scores. We extracted the scores corresponding to the 7,535 cells belonging to cluster 0 (2,984 cells), cluster 1 (2,413 cells) and cluster 2 (2,138 cells) and carried out post-analysis to identify metabolic reactions and subsystems with significantly changed activities when comparing stem-like T_{EP} TEa cells (cluster 0 and 2) versus effector TEa cells (cluster 1). The post-analysis pipeline defined in the original Compass paper were followed[26]. Briefly, the raw penalty scores from Compass were subject to minus natural log transforms to generate activity scores with higher value corresponding to higher metabolic flux/activity. Wilcoxon rank-sum tests with a Benjamini–Hochberg correction for multiple comparisons were applied to identify metabolic reactions with significantly different activity scores between stem-like T_{EP} TEa cells (cluster 0 and 2) and effector TEa cells (cluster 1). Cohen's *d* values were calculated to quantify the effect size for the differences. We focused on a group of 'core reactions', with 3,466 reactions in 91 subsystems as defined in the original Compass paper[26] to further explore the metabolic differences between stem-like T_{EP} TEa cells (cluster 0 and 2) and effector TEa cells (cluster 1). MATLAB R2021b was used to generate dot plots for Cohen's *d* values, corresponding to 1,497 reactions (representing 79 subsystems) with $P \leq 0.05$ between stem-like T_{EP} TEa and effector TEa cells, as well as volcano plots illustrating detailed *P* values and effect sizes for 844 reactions from eight subsystems. We selected a panel of 17 genes and a subset of 57 metabolic reactions and calculated Spearman's correlation coefficients between expression profiles of each gene and activity scores of each reaction across the 7,535 cells. The Morpheus tool from the Broad Institute was used to apply hierarchical clustering on both the genes and metabolic reactions using Euclidean distance and average linkage.

Compass analysis of metabolic states in WT and *Ldha*$^{-/-}$ T_{EP} cells

The clusters of WT and *Ldha*$^{-/-}$ splenic TEa cells are illustrated in Extended Data Fig. 9a. Clusters 0 to 4 were the major stem-like T_{EP} cell clusters, containing 17,841 cells with 11,921 of 17,841 cells being *Ldha*$^{-/-}$ TEa cells. We applied the Compass algorithm[26] and tool with default parameters for metabolic flux modeling using scRNA-seq data from these 17,841 cells from clusters 0 to 4. Each of the 17,841 cells in this dataset was evaluated for the activities of 10,211 metabolic reactions from 99 metabolic subsystems defined in Recon2 model. The Compass tool ran on a MacPro workstation with 4.4 GHz 12-core intel Xeon W processor and 96 GB DDR4 ECC memory and the average time for evaluating one cell was 68.47 s.

The Compass tool produced a matrix with the dimension of 10,211 (reactions) × 17,841 (WT or *Ldha*$^{-/-}$ splenic TEa cells in clusters 0 to 4 in Extended Data Fig. 9a) to record reaction penalty scores. We pooled the scores corresponding to the 11,921 *Ldha*$^{-/-}$ TEa cells and 5,920 WT TEa cells, respectively and carried out post-analysis to identify metabolic reactions and subsystems with significantly changed activities when comparing *Ldha*$^{-/-}$ TEa cells versus WT TEa cells within clusters 0 to 4, defined in Extended Data Fig. 9a. The post-analysis pipeline defined in the original Compass paper were followed[26]. Briefly, the raw penalty scores from Compass were subject to minus natural log transforms to generate activity scores with higher value corresponding to higher metabolic flux/activity. Wilcoxon rank-sum tests with Benjamini–Hochberg correction for multiple comparisons were applied to identify metabolic reactions with significantly different activity scores between *Ldha*$^{-/-}$ TEa cells versus WT TEa cells. Cohen's *d* values were calculated to quantify the effect size for the differences. We focused on a group of 'core reactions', with 3,466 reactions in 91 subsystems as defined in the original Compass paper[26] to further explore the metabolic differences between *Ldha*$^{-/-}$ TEa cells versus WT TEa cells. MATLAB R2021b was used to generate dot plots for Cohen's *d* values corresponding to 1,718 reactions (representing 81 subsystems) with *P* value ≤ 0.05 *Ldha*$^{-/-}$ TEa cells versus WT TEa cells (Extended Data Fig. 9c), as well as volcano plots illustrating detailed *P* values and effect sizes for 93 reactions from four subsystems (Fig. 5f and Extended Data Fig. 9d).

Analysis of human CD4^{+} T cells

Patients with rejected kidney allografts were enrolled at Houston Methodist Hospital between July 2022 and November 2022 in accordance with an approved Houston Methodist Hospital Institutional Review Board protocol. We complied with all relevant ethical regulations. All patients provided informed consent.

Samples from PBMCs and rejected kidney allografts were obtained at the time of nephrectomy of rejected kidneys. Leukocytes were purified from PBMCs using Ficoll density gradient, according to manufacturer's instructions. Kidney allografts were minced into small pieces, washed twice with PBS and then incubated with pre-warm dissociation solution (TrypLE Express Enzyme 1×, Thermo Fisher Scientific) in a shaker at 37 °C for 10 min. The dissociated tissues were mechanically disrupted with a syringe plunger, filtered through a 70-μm cell strainer and collected in cold PBS containing 10% FBS. The cell suspensions were washed twice with PBS containing 2% FBS, followed by removing red blood cells with ACK lysis buffer. Flow cytometry was used to determine the TCF1 expression in CXCR6^{+} or CXCR6^{-} graft-infiltrating CD4^{+} T cells as well as in CXCR6^{-}CD4^{+} T cells from PBMCs. CXCR6^{+} and CXCR6^{-}CD4^{+} T cells from kidney allografts and PBMCs were sorted, labeled with CTV and stimulated with or without Dynabeads Human T-Activator CD3/CD28 (Thermo Fisher) in 96-well plates (2.5×10^4 cells per well), followed by flow cytometric analysis on day 4 after simulation.

Statistical analysis

Statistical analyses were performed using two-tailed unpaired Student's *t*-test and log-rank test (Prism 8.0.0, GraphPad Software) unless otherwise indicated. $P < 0.05$ was considered statistically significant. No statistical methods were used to predetermine sample sizes but

our sample sizes are similar to those reported in previous publications[29,36]. Data distribution was assumed to be normal but this was not formally tested. Age- and sex-matched mice with predetermined genotypes were randomly assigned for experiments. No other randomization was performed. Data collection and analysis were not performed blind to the conditions of the experiments. No animals or data points were excluded from the analyses.

Extended Data

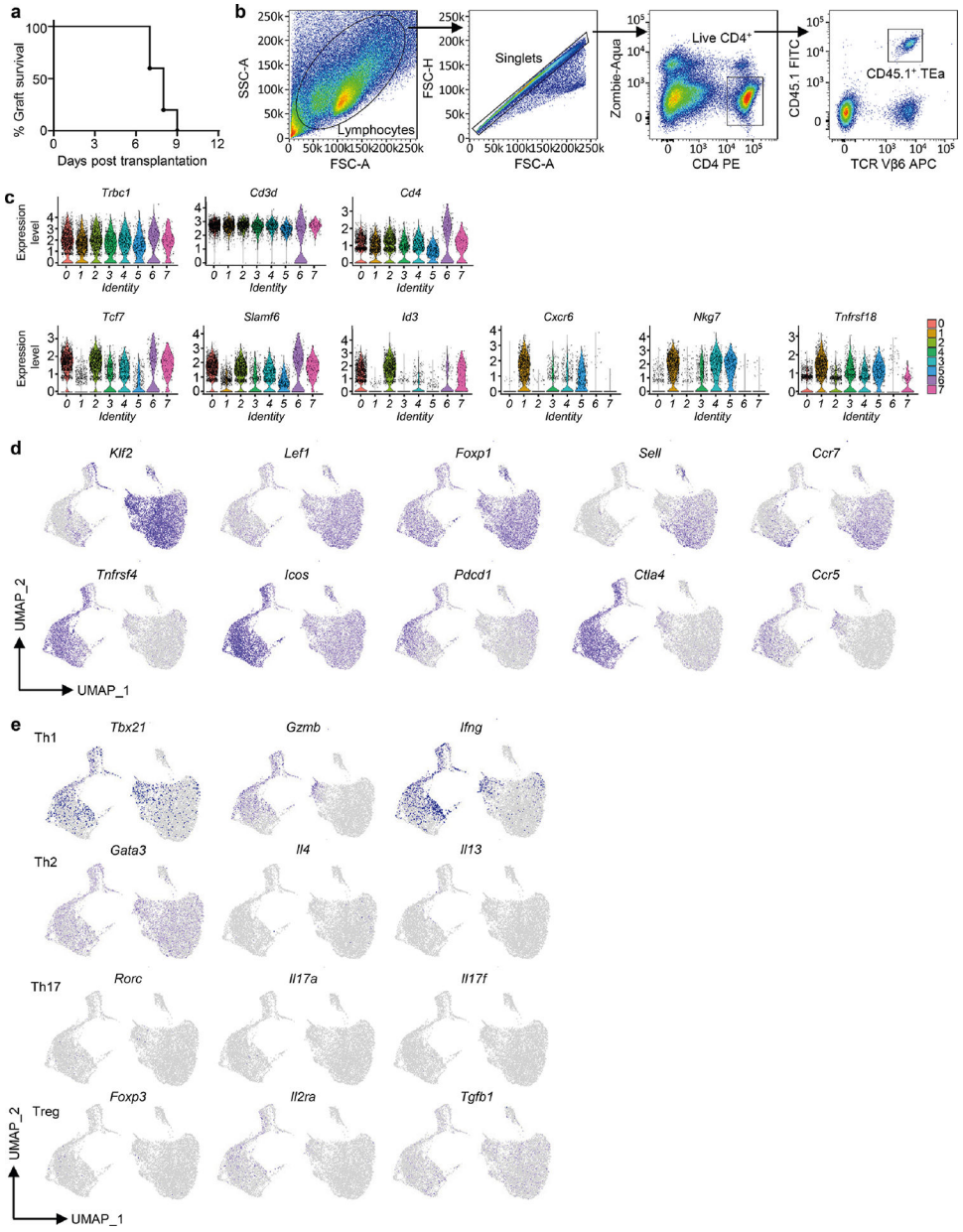

Extended Data Fig. 1 |. Single-cell transcriptome analysis of alloreactive CD4$^+$ T cells (related to Fig. 1).

a–e, CD45.2$^+$ WT B6 mice were adoptively transferred with CD45.1$^+$ TEa CD4$^+$ T cells, followed by BALB/c heart transplantation 1 d later. The transferred TEa cells from

spleens and heart allografts were obtained at 7 days post-transplantation for scRNA-seq. **a**, Percentage heart allograft survival after transplantation. $n = 5$ mice. **b**, The gating strategy for sorting the transferred TEa cells from recipients. **c**, Violin plots show the expression distributions of indicated T cell marker genes, stem-like genes, and effector genes in each of the TEa cell clusters. **d**, Feature plots show the normalized gene expression of stem-like T_{EP} cell and effector cell markers projected onto the uniform manifold approximation and projection (UMAP). **e**, Feature plots show the normalized gene expression of Th1, Th2, Th17, and Treg cell markers, projected onto the UMAP. In both **d** and **e**, gene expression level represented by color gradient ranging from gray (low expression) to purple (high expression).

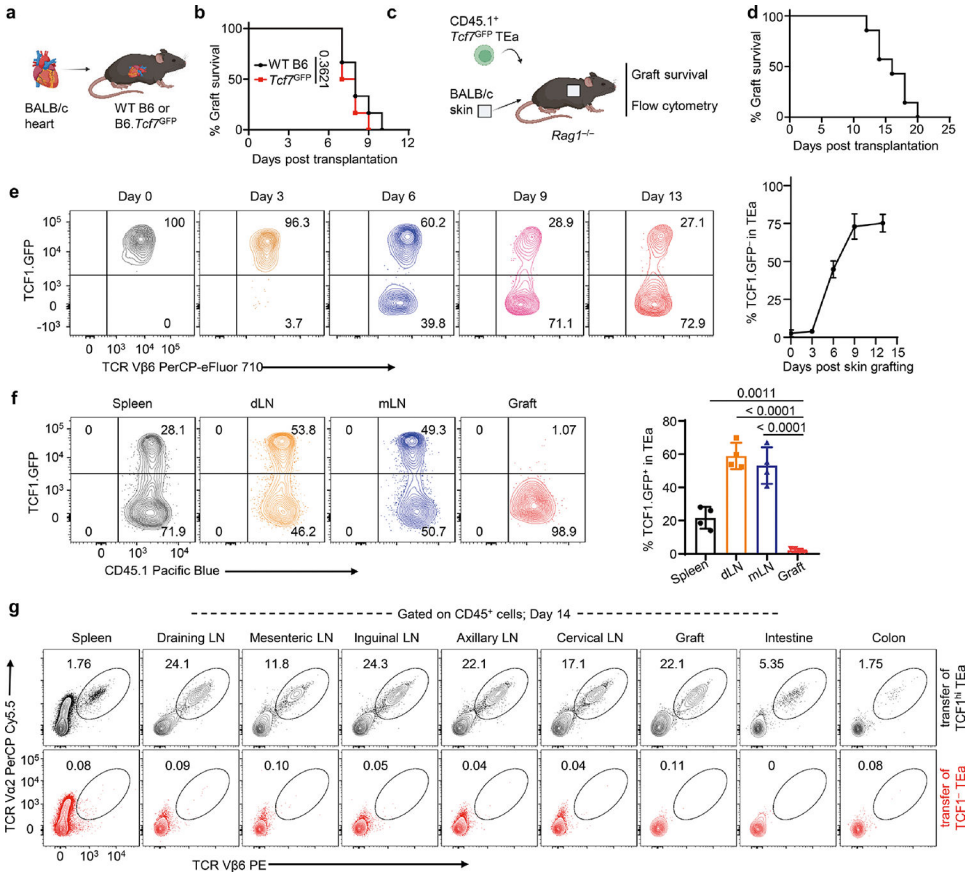

Extended Data Fig. 2 |. Phenotypic characterization of the adoptively transferred TEa CD4$^+$ T cells in transplant recipients (related to Figs. 2 and 3).

a,**b**, WT B6 and B6.*Tcf7*^{GFP} mice were transplanted with BALB/c hearts. **a**, Experimental scheme. **b**, Percentage heart allografts in WT B6 and B6.*Tcf7*^{GFP} mice ($n = 6$ mice per group). **c–f**, B6.*Rag1*$^{-/-}$ mice were adoptively transferred with CD45.1$^+$ *Tcf7*^{GFP} TEa cells and transplanted with BALB/c skins. **c**, Experimental scheme. **d**, Percentage skin allograft survival. $n = 7$ mice. **e**, TCF1.GFP expression of TEa cells in blood at indicated days after transplantation. Flow plots are gated on TEa cells. The line graph shows percentages of TCF1.GFP$^-$ cells in TEa cells. Data are mean ± SD ($n = 8$ mice). **f**, TCF1.GFP expression of TEa cells in indicated tissues at 14 days after transplantation. Flow plots are gated on TEa

cells. The bar graph shows percentages of TCF1.GFP$^+$ cells in TEa cells. Data are mean ± SD (n = 4 mice), and results are representative of two independent experiments. **g**, CD45.1$^+$ *Tcf7*^{GFP} TEa cells were adoptively transferred into *Rag1*$^{-/-}$ mice receiving BALB/c skin transplantation. At 14 days post-transplantation, TCF1^{hi} and TCF1$^-$ TEa cells were isolated from the secondary lymphoid organs and transferred into new *Rag1*$^{-/-}$ hosts that received BALB/c skin transplantation. In these new hosts, representative flow plots show TEa cell frequencies among CD45$^+$ cells in indicated organs 14 days post-transplantation (related to Fig. 3e). In **a** and **c**, experimental schemes were created with BioRender.com. *P* values are from two-tailed unpaired Student's *t*-test (**f**) or log-rank test (**b**).

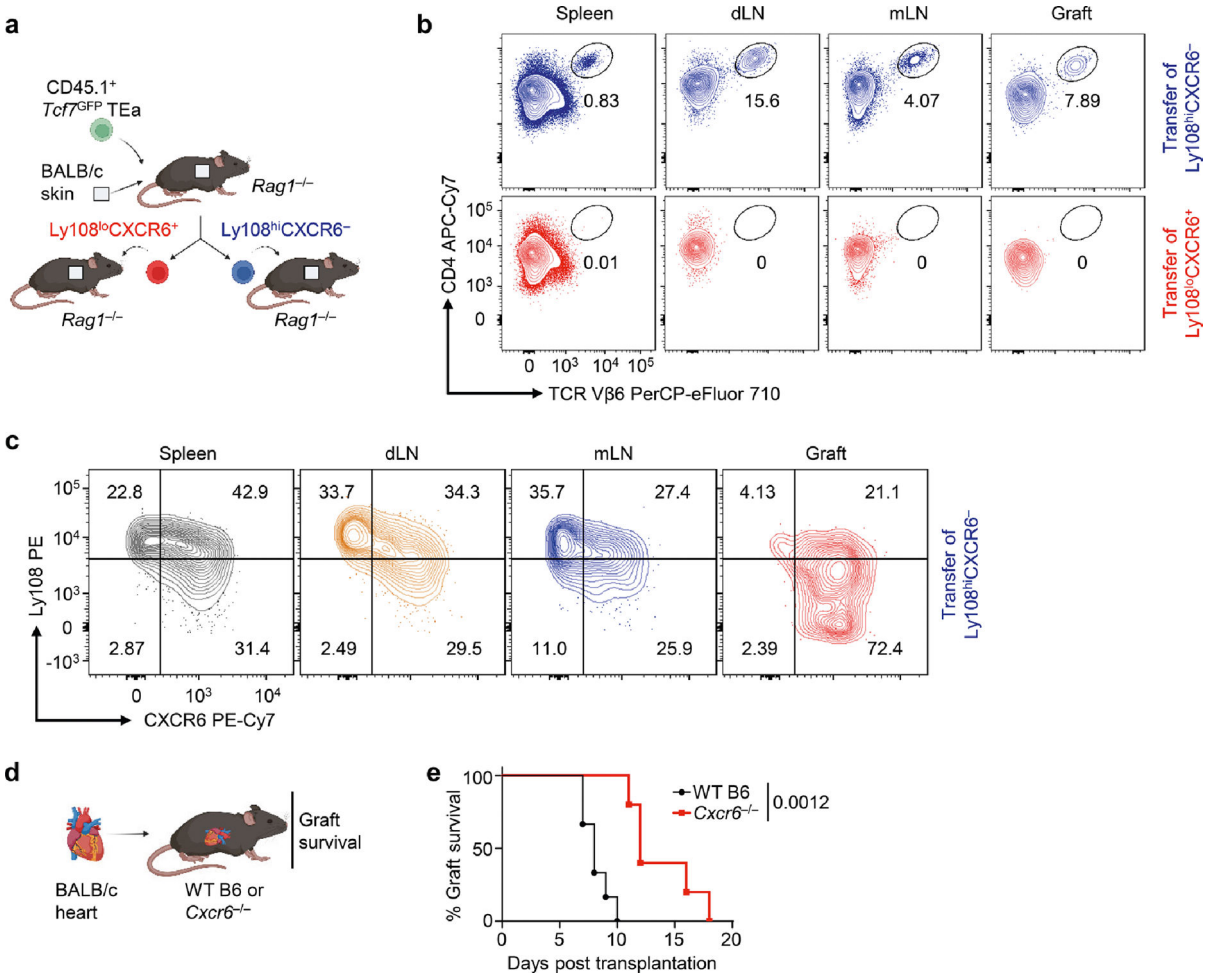

Extended Data Fig. 3 |. CD4$^+$ T_{EP} cells self-renew and replenish the effector cell pool. **a–c**, CD45.1$^+$ *Tcf7*^{GFP} TEa cells were adoptively transferred into *Rag1*$^{-/-}$ recipients receiving BALB/c skin transplantation. Ly108^{hi}CXCR6$^-$ T_{EP} TEa and Ly108^{lo}CXCR6$^+$ effector TEa cells were isolated from the spleens and lymph nodes at 14 days post-transplantation, and adoptively transferred into new *Rag1*$^{-/-}$ recipients receiving BALB/c skin transplantation. The phenotypic changes of T_{EP} TEa and effector TEa cells in new recipients were analyzed at 14 days post-transplantation. **a**, Experimental scheme. **b**, Representative flow plots (related to Fig. 3j) show percentage TEa cells within CD45$^+$

cells in new recipients that were transferred with Ly108^{hi}CXCR6^{-} or Ly108^{lo}CXCR6^{+} TEa cells. Flow plots are gated on CD45^{+} cells. **c**, Representative flow plots (related to Fig. 3k) show Ly108 and CXCR6 expression of TEa cells in new recipients that were transferred with Ly108^{hi}CXCR6^{-} T_{EP} TEa cells. Flow plots are gated on TEa cells. **d**,**e**, *Cxcr6*$^{-/-}$ and WT B6 mice were transplanted with BALB/c hearts. **d**, Experimental scheme. **e**, Percentage heart allograft survival after transplantation. *n* = 6 mice for the WT group, and *n* = 5 mice for the *Cxcr6*$^{-/-}$ group. In **a** and **d**, experimental schemes were created with BioRender.com. The *P* value is from log-rank test (**e**).

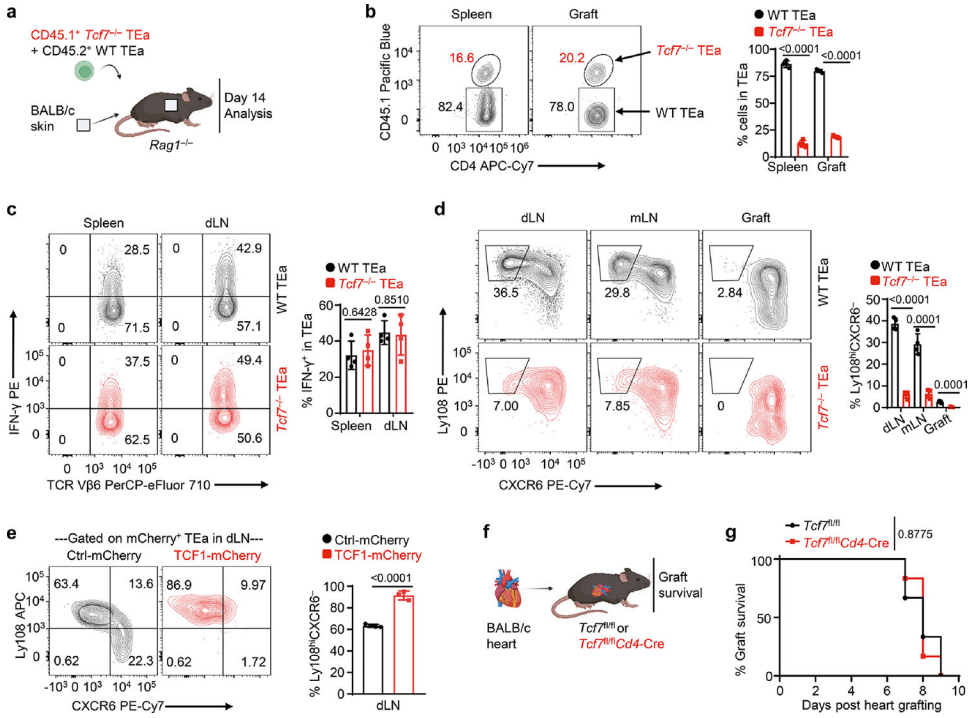

Extended Data Fig. 4 |. TCF1 sustains stem-like CD4^{+} T_{EP} cells (related to Fig. 4).
a–d, CD45.1^{+} *Tcf7*$^{-/-}$ TEa and CD45.2^{+} WT TEa cells were mixed in a 1:1 ratio and adoptively co-transferred into *Rag1*$^{-/-}$ mice, followed by BALB/c skin transplantation. TEa cells in recipients were analyzed at 14 days post-transplantation. **a**, Experimental scheme. **b**, Percentage *Tcf7*$^{-/-}$ TEa and WT TEa cells among total TEa cells in spleens and grafts. *n* = 4 mice. **c**, IFN-γ production by *Tcf7*$^{-/-}$ TEa and WT TEa cells in spleens and dLNs. *n* = 4 mice. **d**, Percentage Ly108^{hi}CXCR6^{-} cells within *Tcf7*$^{-/-}$ TEa or WT TEa cells in the indicated tissues. *n* = 4 mice. Flow plots in **b–d** are gated on TEa cells. **e**, *Rag1*$^{-/-}$ mice were adoptively transferred with WT TEa cells transduced with mCherry alone (Ctrl-mCherry) or TCF1-mCherry, followed by BALB/c skin transplantation. Representative flow plots show Ly108 and CXCR6 expression of mCherry^{+} TEa cells in dLN at 14 days post-transplantation. Flow plots are gated on mCherry^{+} TEa cells. The bar graph shows percentage Ly108^{hi}CXCR6^{+} cells in mCherry^{+} TEa cells. *n* = 4 mice for the Ctrl-mCherry group, and *n* = 3 mice for the TCF1-mCherry group. **f**,**g**, *Tcf7*$^{fl/fl}$*Cd4*-Cre and *Tcf7*$^{fl/fl}$ control mice were transplanted with BALB/c hearts. **f**, Experimental scheme. **g**, Percentage heart allograft survival after transplantation. *n* = 6 mice per group. In **a** and **f**, experimental

schemes were created with BioRender.com. In **b–e**, data are presented as mean ± SD, and results are representative of two independent experiments. *P* values are from two-tailed unpaired Student's *t*-test (**b–e**) or log-rank test (**g**).

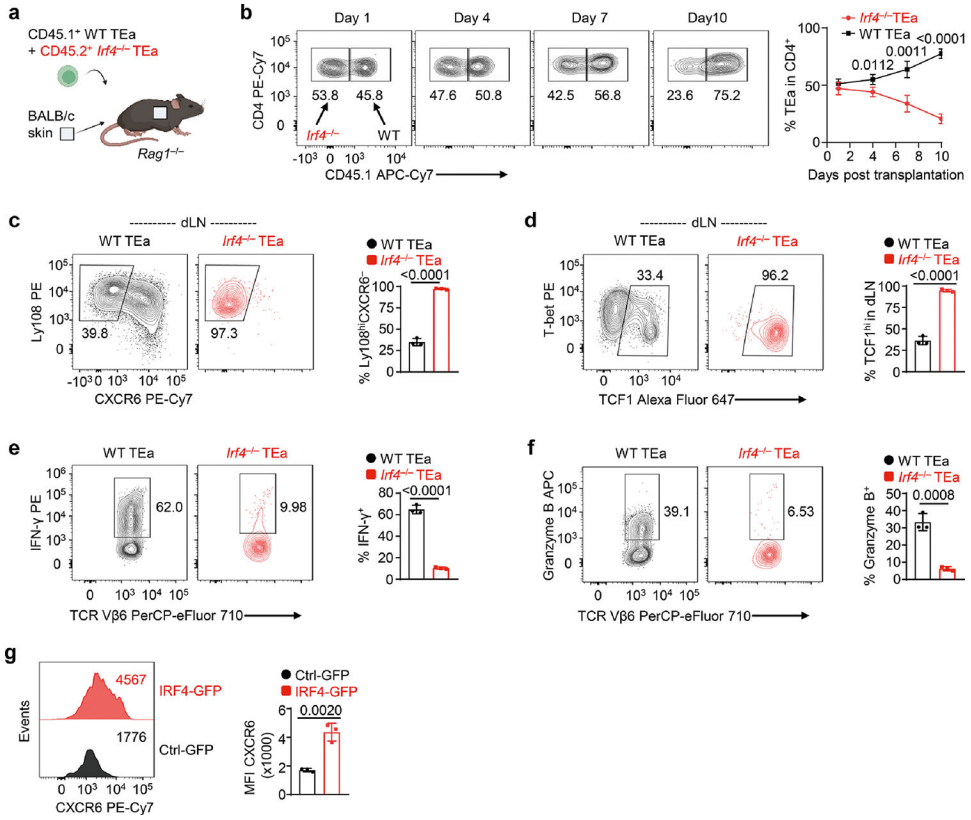

Extended Data Fig. 5 |. IRF4 governs the effector differentiation potential of stem-like CD4$^+$ T_{EP} cells (related to Fig. 4).

a–f, *Rag1*$^{-/-}$ mice were adoptively co-transferred with CD45.2$^+$ *Irf4*$^{-/-}$ TEa and CD45.1$^+$ WT TEa cells (in a 1:1 ratio), followed by BALB/c skin transplantation. **a**, Experimental scheme. Created with BioRender.com. **b**, Percentage *Irf4*$^{-/-}$ TEa and WT TEa cells within total TEa cells in blood at indicated days post-transplantation. Flow plots are gated on TEa cells. $n = 4$ mice. **c**, Representative flow plots show Ly108 and CXCR6 expression of TEa cells in dLN at 14 days post-transplantation. The bar graph shows percentage Ly108^{hi}CXCR6$^-$ cells in *Irf4*$^{-/-}$ TEa and WT TEa cells. $n = 3$ mice. **d**, Percentage of TCF1$^+$ cells within *Irf4*$^{-/-}$ TEa and WT TEa cells in the dLN at 14 days post-transplantation. $n = 3$ mice. **e**, Percentage of IFN-γ$^+$ cells among *Irf4*$^{-/-}$ TEa and WT TEa cells in the dLN at 14 days post-transplantation. $n = 3$ mice. **f**, Percentage of granzyme B$^+$ cells among *Irf4*$^{-/-}$ TEa and WT TEa cells in the dLN at 14 days post-transplantation. $n = 3$ mice. **g**, *Rag1*$^{-/-}$ mice were adoptively transferred with *Irf4*$^{-/-}$ TEa cells transduced with GFP alone (Ctrl–GFP) or IRF4–GFP, followed by BALB/c skin transplantation. Histogram and bar graph show CXCR6 expression of GFP$^+$ TEa cells in the dLN at 14 days post-transplantation. $n = 3$ mice per group. In **b–g**, data are mean ± SD. *P* values are from two-tailed unpaired Student's *t*-test (**b–g**).

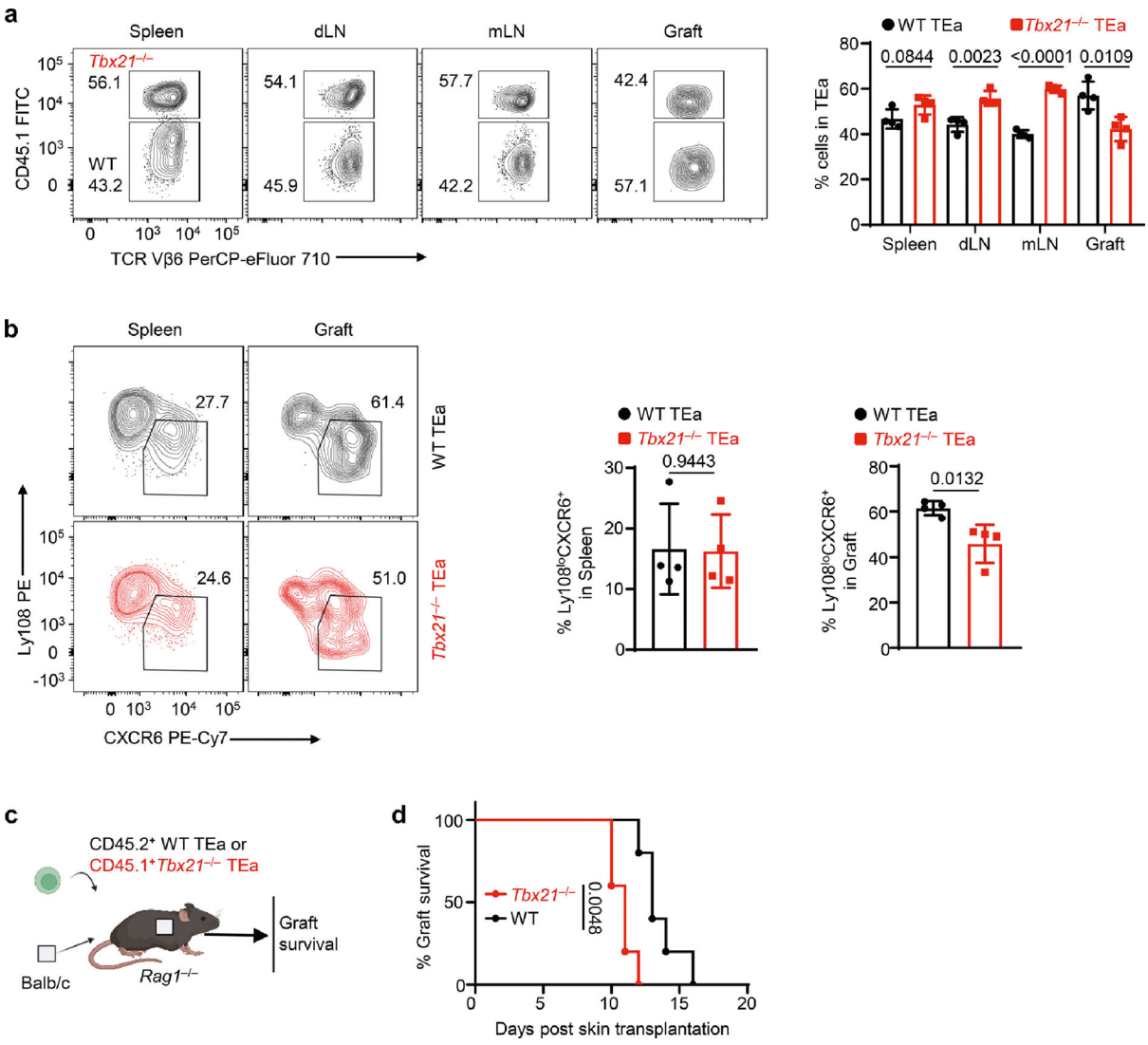

Extended Data Fig. 6 |. T-bet is dispensable for the generation of Ly108^{lo}CXCR6^{+} effectors. **a–b**, *Rag1*$^{-/-}$ mice were adoptively co-transferred with CD45.1^{+} *Tbx21*$^{-/-}$ TEa and CD45.2^{+} WT TEa cells (in a 1:1 ratio), followed by BALB/c skin transplantation. The transferred TEa cells were analyzed at 14 days post-transplantation. **a**, Percentage *Tbx21*$^{-/-}$ TEa and WT TEa cells within total TEa cells in indicated tissues. Flow plots are gated on TEa cells. $n = 4$ mice. **b**, Percentage Ly108^{lo}CXCR6^{+} cells in *Tbx21*$^{-/-}$ TEa and WT TEa cells. Flow plots are gated on WT TEa or *Tbx21*$^{-/-}$ TEa cells. $n = 4$ mice. **c**,**d**, *Rag1*$^{-/-}$ mice were adoptively transferred with *Tbx21*$^{-/-}$ TEa or WT TEa cells, followed by BALB/c skin transplantation. **c**, Experimental scheme. Created with BioRender.com. **d**, Percentage allograft survival. $n = 5$ mice per group. In **a**,**b**, data are mean ± SD, and results are representative of two independent experiments. *P* values are from two-tailed unpaired Student's *t*-test (**a**,**b**) or log-rank test (**d**).

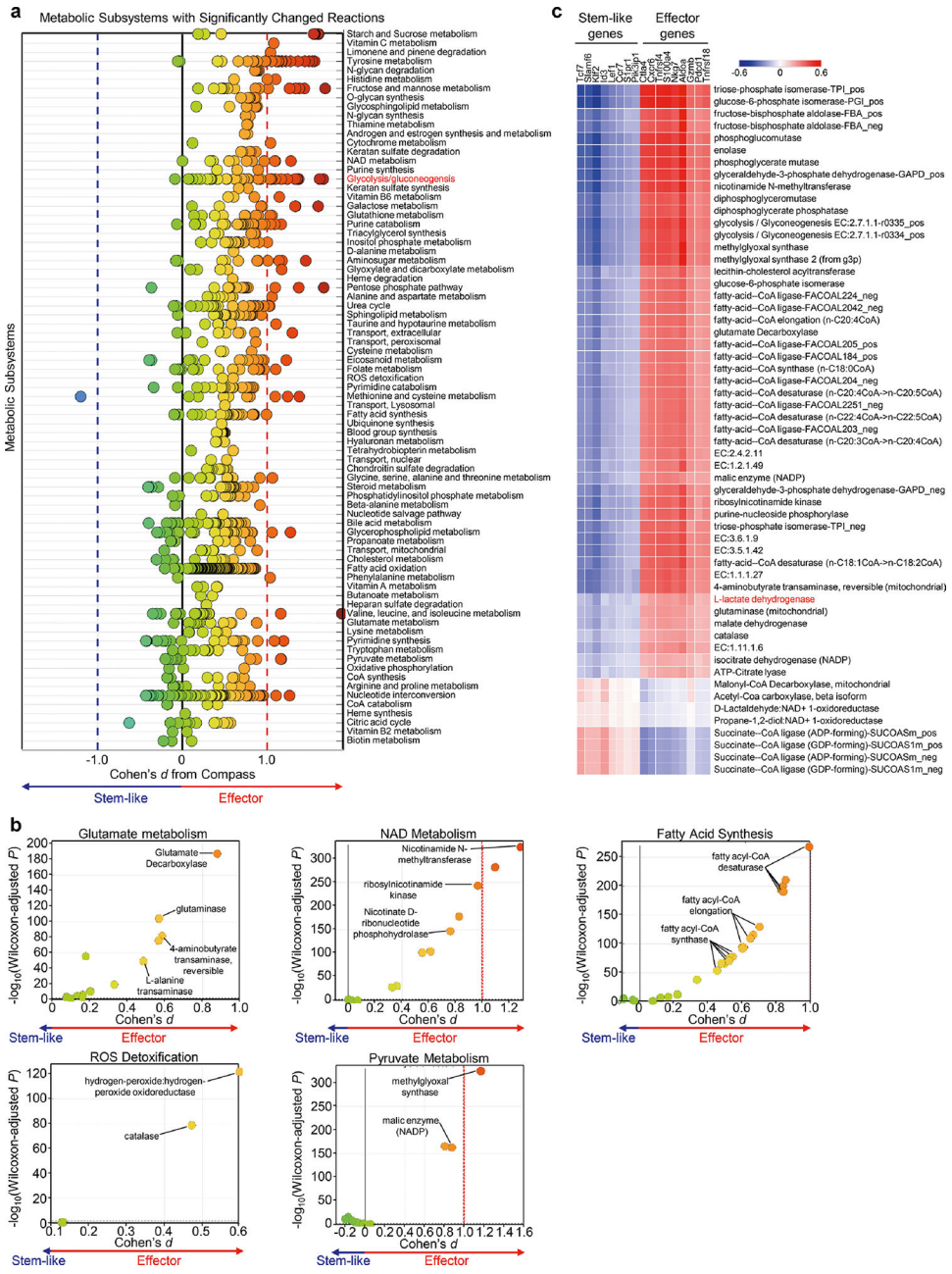

Extended Data Fig. 7 |. Identification of metabolic reactions that are significantly differentially active in stem-like T_{EP} or effector $CD4^+$ T cells.

a–c, Compass algorithm was applied to analyze the metabolic states of alloantigen-specific TEa cells, based on scRNA-seq data. **a**, Differential activity of 1,497 reactions (colored dots) in 79 metabolic subsystems when compared between stem-like T_{EP} TEa and effector TEa cells. Cohen′s *d* was used to determine the effect sizes. **b**, Volcano plots illustrate the detailed *P* values and effect sizes for metabolic reactions in 5 indicated subsystems when compared between stem-like T_{EP} TEa and effector TEa cells. **c**, Spearman correlation of Compass scores with the expression of stem-like genes or effector genes. Rows are metabolic reactions selected from 8 subsystems listed in **b** and Fig. 5a–c. In **b**, data were

analyzed by two-sided Wilcoxon rank-sum tests with Benjamini–Hochberg correction for multiple comparisons.

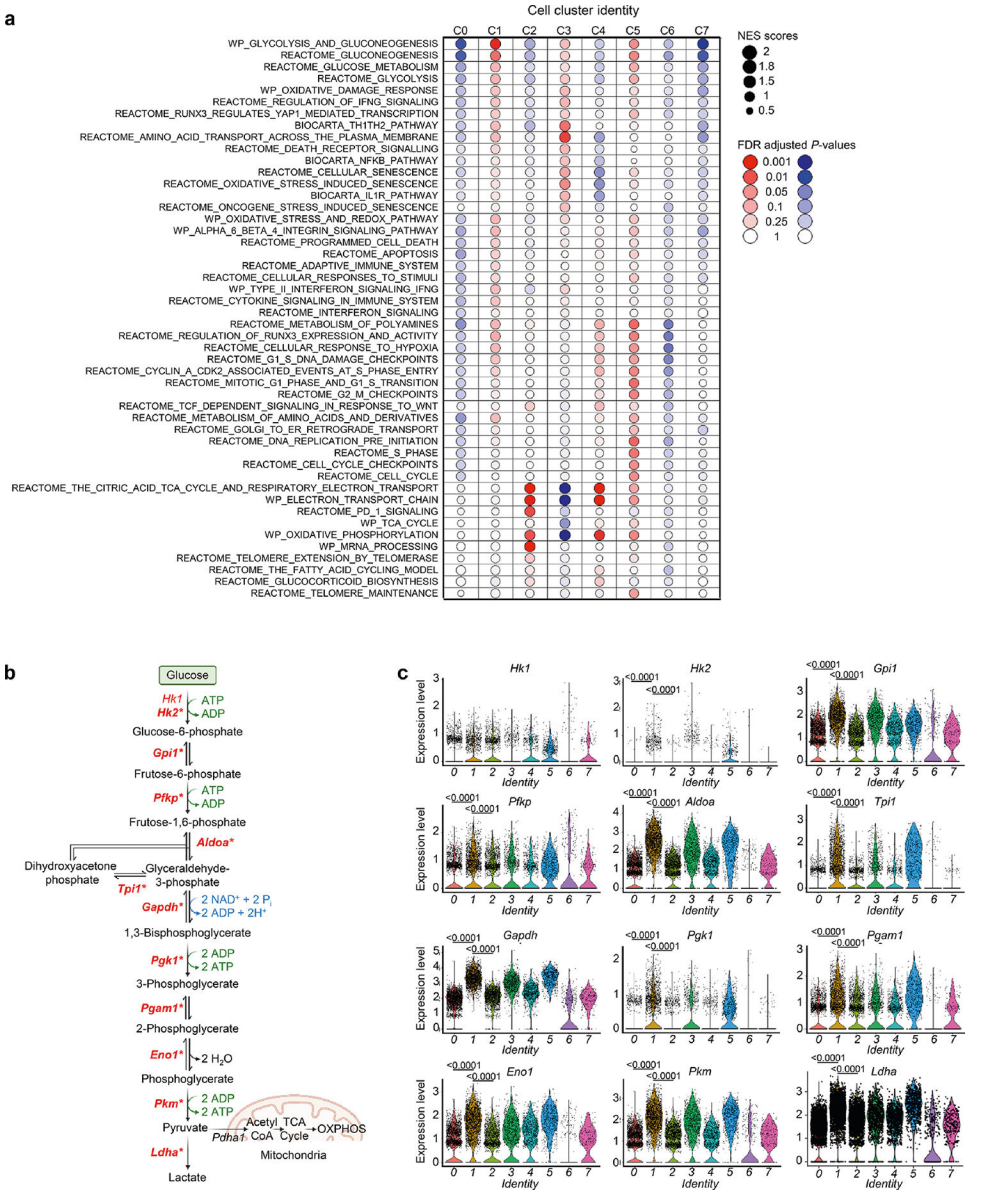

Extended Data Fig. 8 |. Enhanced glycolytic metabolism in CD4$^+$ effector T cells.

a, Gene set enrichment analysis (GSEA) of scRNA-seq data identifies 801 pathways that are differentially expressed in TEa cell clusters. The bubble plot illustrates 48 representative pathways in each TEa cell cluster. Node sizes are proportional to NES scores from GSEA. Red color indicates upregulation in one cluster when compared to all other clusters. Blue color indicates downregulation in one cluster when compared to all other clusters. Color intensities correspond to FDR adjusted *P* values from GSEA. **b**, Schematic depicting the critical enzymes that catalyze sequential reactions in glycolysis. Adapted from 'Glycolysis and Glycolytic Enzymes', by BioRender.com (2023). Retrieved from https://app.biorender.com/biorender-templates. Genes significantly upregulated in effector (cluster

1) versus T_{EP} (clusters 0 and 2) TEa cells were marked in bold red font with an asterisk. **c**, Violin plots show the expression distributions of indicated genes (encoding glycolytic enzymes) in each TEa cell clusters. In **a**, data were analyzed by weighted Kolmogorov-Smirnov tests, and false discovery rates (FDR) were calculated. In **c**, data were analyzed by two-sided Wilcoxon rank-sum tests with Bonferroni correction for multiple comparisons.

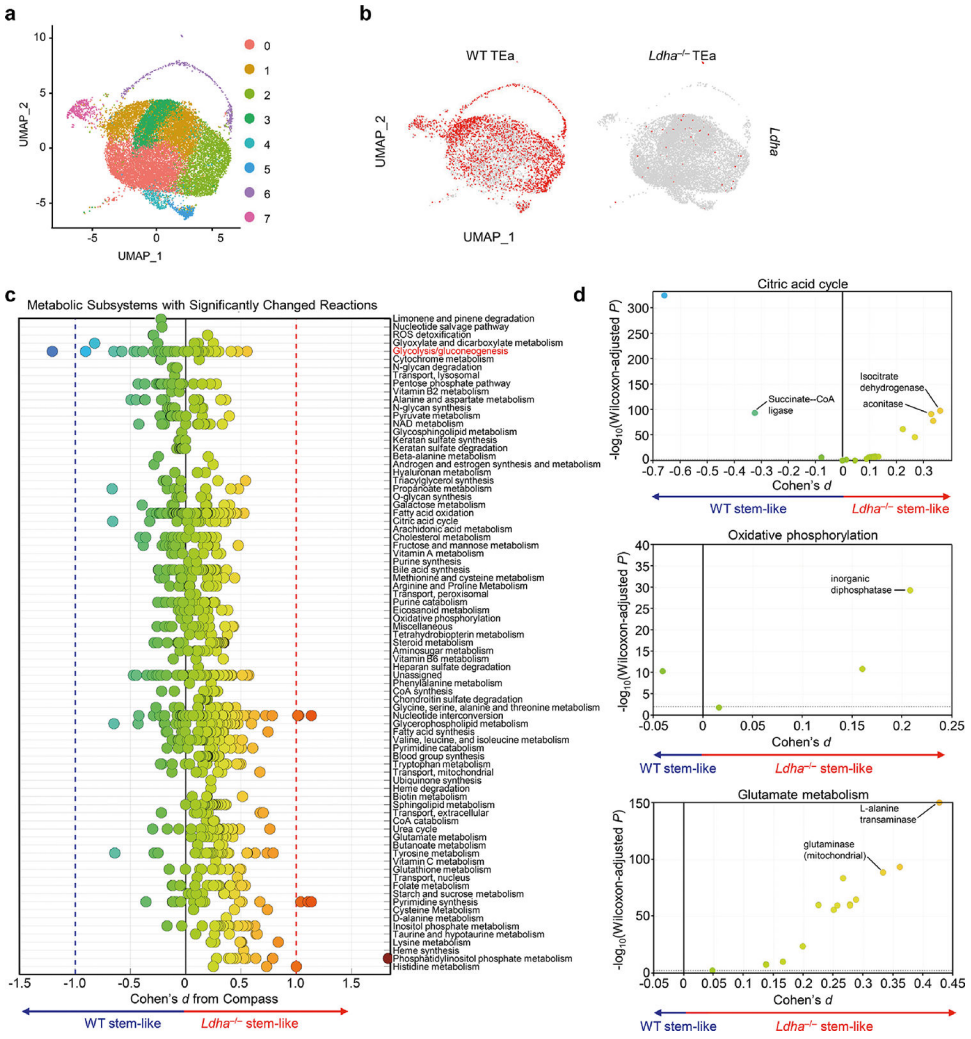

Extended Data Fig. 9 |. scRNA-seq identifies LDHA as a crucial regulator of effector differentiation of T_{EP} cells.

a–d, On day 7 post-heart transplantation, transferred WT TEa and *Ldha*$^{-/-}$ TEa cells were isolated from recipient spleens for scRNA-seq analysis. **a**, UMAP analysis of TEa cells, including both WT TEa and *Ldha*$^{-/-}$ TEa cells from recipient spleens. Distinct color schemes were used to identify and visually represent the eight clusters (0–7). **b**, Feature plots project normalized *Ldha* gene expression onto the UMAPs for WT TEa or *Ldha*$^{-/-}$ TEa cell population. **c,d**, The compass algorithm was used to assess the metabolic states of WT stem-like and *Ldha*$^{-/-}$ stem-like TEa cells. **c**, Differential activity of metabolic reactions (colored dots) in metabolic subsystems between WT stem-like and *Ldha*$^{-/-}$ stem-like TEa cells, with Cohen's *d* determining the effect sizes. **d**, Volcano plots

illustrate the detailed *P* values and effect sizes for metabolic reactions in the citric acid cycle, oxidative phosphorylation, and glutamate metabolism. In **d**, data were analyzed by two-sided Wilcoxon rank-sum tests with Benjamini–Hochberg correction for multiple comparisons.

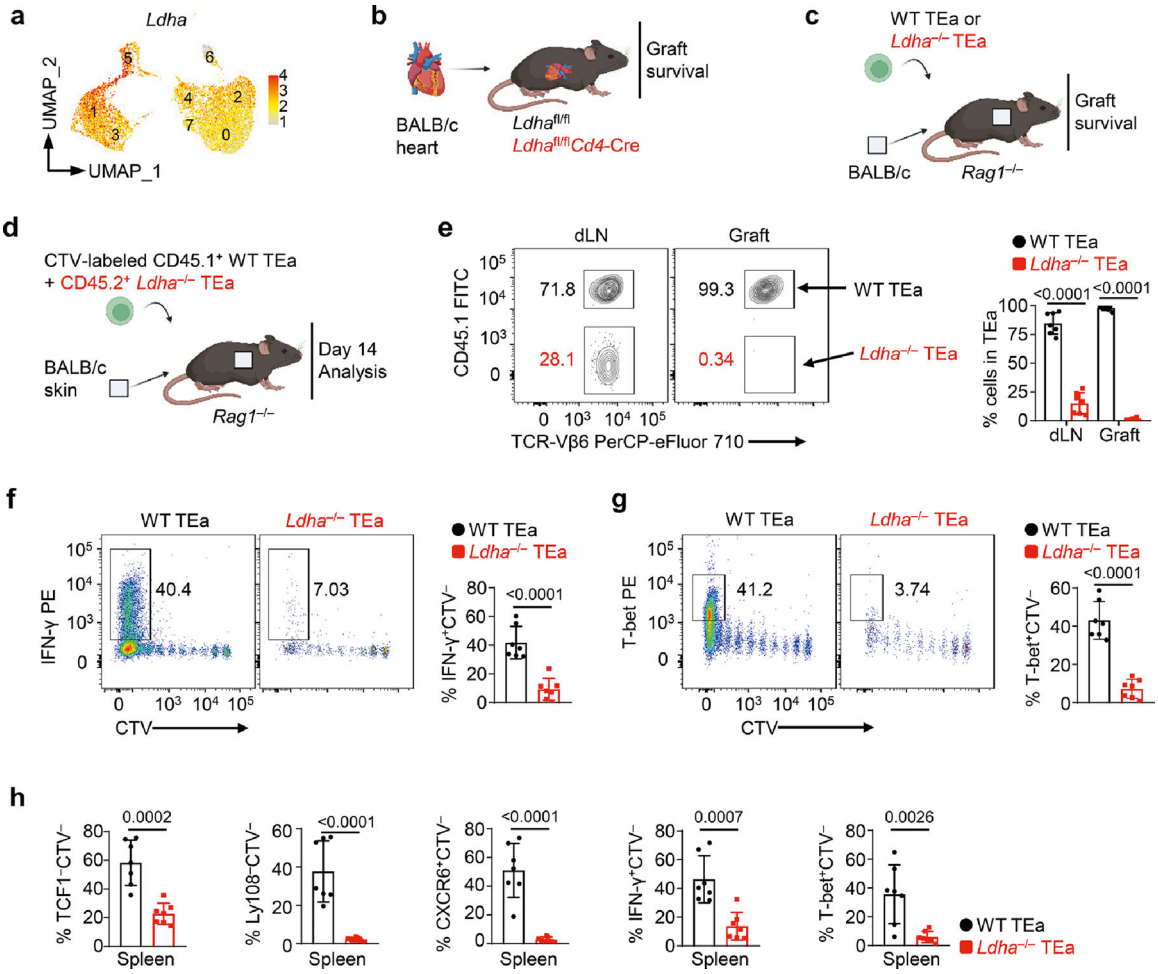

Extended Data Fig. 10 |. LDHA governs the effector differentiation potential of CD4$^+$ T_{EP} cells. **a**, The UMAP feature plot shows normalized *Ldha* expression. Cluster numbers (related to Fig. 1b) are indicated in the UMAP plot. **b**, Experimental scheme for Fig. 6a. **c**, Experimental scheme for Fig. 6b. **d–h**, CD45.1$^+$ WT TEa and CD45.2$^+$ *Ldha*$^{-/-}$ TEa cells were mixed in a 1:1 ratio, labeled with CTV, and adoptively co-transferred into *Rag1*$^{-/-}$ mice 1 d before BALB/c skin transplantation. The transferred TEa cells were analyzed by flow cytometry on day 14 post-skin transplantation. **d**, Experimental scheme. **e**, Percentage of WT TEa and *Ldha*$^{-/-}$ TEa cells among total TEa cells in dLNs and grafts. Flow plots are gated on TEa cells. $n = 7$ mice. **f**,**g**, Representative flow plots and bar graphs show % IFNγ^+CTV$^-$ (**f**; $n = 7$ mice) and T-bet$^+$CTV$^-$ (**g**; $n = 7$ mice) TEa cells among the transferred WT or *Ldha*$^{-/-}$ TEa cells in dLNs. **h**, Bar graphs show % TCF1$^-$CTV$^-$, Ly108$^-$CTV$^-$, CXCR6$^+$CTV$^-$, IFNγ^+CTV$^-$, and T-bet$^+$CTV$^-$ TEa cells among the transferred WT or *Ldha*$^{-/-}$ TEa cells in spleens. $n = 7$ mice. In **b–d**, experimental

schemes were created with BioRender.com. In **e–h**, data are mean ± SD, and results are pooled from two independent experiments. *P* values are from two-tailed unpaired Student's *t*-test (**e–h**).

Acknowledgements

This study was supported by internal funding from Houston Methodist Research Institute (to W.C. and S.G.Y.) and the US National Institutes of Health grants (R01 AI132492 to W.C. and R01 AI129906 to X.C.L.). The authors thank the staff at the Single Cell Genomics Core at Baylor College of Medicine (partially supported by the National Institutes of Health shared instrument grants (S10OD023469 and S10OD025240), P30EY002520 and CPRIT grant RP200504), the Biostatistics and Bioinformatics shared resources at Houston Methodist Neal Cancer Center and the Houston Methodist Flow Cytometry Core Facility for excellent services. Schematic diagrams of experimental design were created with BioRender.com.

Data availability

The scRNA-seq data have been deposited in the Gene Expression Omnibus under accession no. GSE221337. Raw Illumina sequencing reads of scRNA-seq datasets were aligned to reference mouse genome mm10 (Ensembl 93), http://jul2018.archive.ensembl.org/Mus_musculus/Info/Index. All other data supporting the findings of this study are available within the article and supplementary information. Source data are provided with this paper.

References

1. Pawlak M, Ho AW & Kuchroo VK Cytokines and transcription factors in the differentiation of CD4(+) T helper cell subsets and induction of tissue inflammation and autoimmunity. Curr. Opin. Immunol. 67, 57–67 (2020). [PubMed: 33039897]
2. Ruterbusch M, Pruner KB, Shehata L & Pepper M In vivo CD4(+) T cell differentiation and function: revisiting the Th1/Th2 paradigm. Annu. Rev. Immunol. 38, 705–725 (2020). [PubMed: 32340571]
3. Smith-Garvin JE, Koretzky GA & Jordan MS T cell activation. Annu. Rev. Immunol. 27, 591–619 (2009). [PubMed: 19132916]
4. Schnell A et al. Stem-like intestinal Th17 cells give rise to pathogenic effector T cells during autoimmunity. Cell 184, 6281–6298 (2021). [PubMed: 34875227]
5. Xia Y et al. BCL6-dependent TCF-1(+) progenitor cells maintain effector and helper CD4(+) T cell responses to persistent antigen. Immunity 55, 1200–1215 (2022). [PubMed: 35637103]
6. Zhou X et al. Differentiation and persistence of memory CD8(+) T cells depend on T cell factor 1. Immunity 33, 229–240 (2010). [PubMed: 20727791]
7. Goldman N et al. Intrinsically disordered domain of transcription factor TCF-1 is required for T cell developmental fidelity. Nat. Immunol. 10.1038/s41590-023-01599-7 (2023).
8. Choi YS et al. LEF-1 and TCF-1 orchestrate T(FH) differentiation by regulating differentiation circuits upstream of the transcriptional repressor Bcl6. Nat. Immunol. 16, 980–990 (2015). [PubMed: 26214741]
9. Im SJ et al. Defining $CD8^+$ T cells that provide the proliferative burst after PD-1 therapy. Nature 537, 417–421 (2016). [PubMed: 27501248]
10. Utzschneider DT et al. T cell factor 1-expressing memory-like CD8(+) T cells sustain the immune response to chronic viral infections. Immunity 45, 415–427 (2016). [PubMed: 27533016]
11. Wu T et al. The TCF1-Bcl6 axis counteracts type I interferon to repress exhaustion and maintain T cell stemness. Sci. Immunol. 1, eaai8593 (2016). [PubMed: 28018990]
12. Gray SM, Amezquita RA, Guan T, Kleinstein SH & Kaech SM Polycomb repressive complex 2-mediated chromatin repression guides effector CD8(+) T cell terminal differentiation and loss of multipotency. Immunity 46, 596–608 (2017). [PubMed: 28410989]

13. Man K et al. The transcription factor IRF4 is essential for TCR affinity-mediated metabolic programming and clonal expansion of T cells. Nat. Immunol. 14, 1155–116 (2013). [PubMed: 24056747]
14. Bollig N et al. Transcription factor IRF4 determines germinal center formation through follicular T-helper cell differentiation. Proc. Natl Acad. Sci. USA 109, 8664–8669 (2012). [PubMed: 22552227]
15. Brustle A et al. The development of inflammatory T(H)-17 cells requires interferon-regulatory factor 4. Nat. Immunol. 8, 958–966 (2007). [PubMed: 17676043]
16. Staudt V et al. Interferon-regulatory factor 4 is essential for the developmental program of T helper 9 cells. Immunity 33, 192–202 (2010). [PubMed: 20674401]
17. Yao S et al. Interferon regulatory factor 4 sustains CD8(+) T cell expansion and effector differentiation. Immunity 39, 833–845 (2013). [PubMed: 24211184]
18. Honma K et al. Interferon regulatory factor 4 differentially regulates the production of Th2 cytokines in naive vs. effector/memory CD4+ T cells. Proc. Natl Acad. Sci. USA 105, 15890–15895 (2008). [PubMed: 18836070]
19. Spiljar M & Kuchroo VK Metabolic regulation and function of T helper cells in neuroinflammation. Semin. Immunopathol. 44, 581–598 (2022). [PubMed: 36068310]
20. Wang R & Green DR Metabolic checkpoints in activated T cells. Nat. Immunol. 13, 907–915 (2012). [PubMed: 22990888]
21. Claps G et al. The multiple roles of LDH in cancer. Nat. Rev. Clin. Oncol. 19, 749–762 (2022). [PubMed: 36207413]
22. Peng M et al. Aerobic glycolysis promotes T helper 1 cell differentiation through an epigenetic mechanism. Science 354, 481–484 (2016). [PubMed: 27708054]
23. Xu K et al. Glycolytic ATP fuels phosphoinositide 3-kinase signaling to support effector T helper 17 cell responses. Immunity 54, 976–987 (2021). [PubMed: 33979589]
24. Xu K et al. Glycolysis fuels phosphoinositide 3-kinase signaling to bolster T cell immunity. Science 371, 405–410 (2021). [PubMed: 33479154]
25. Angelin A et al. Foxp3 reprograms T cell metabolism to function in low-glucose, high-lactate environments. Cell Metab. 25, 1282–1293 (2017). [PubMed: 28416194]
26. Wagner A et al. Metabolic modeling of single Th17 cells reveals regulators of autoimmunity. Cell 184, 4168–4185 (2021). [PubMed: 34216539]
27. Bolton EM, Gracie JA, Briggs JD, Kampinga J & Bradley JA Cellular requirements for renal allograft rejection in the athymic nude rat. J. Exp. Med. 169, 1931–1946 (1989). [PubMed: 2659723]
28. Krieger NR, Yin DP & Fathman CG $CD4^+$ but not $CD8^+$ cells are essential for allorejection. J. Exp. Med. 184, 2013–2018 (1996). [PubMed: 8920888]
29. Wu J et al. Ablation of transcription factor IRF4 promotes transplant acceptance by driving allogenic CD4(+) T cell dysfunction. Immunity 47, 1114–1128 (2017). [PubMed: 29221730]
30. Liu Z, Fan H & Jiang S CD4(+) T-cell subsets in transplantation. Immunol. Rev. 252, 183–191 (2013). [PubMed: 23405905]
31. Conlon TM et al. Germinal center alloantibody responses are mediated exclusively by indirect-pathway CD4 T follicular helper cells. J. Immunol. 188, 2643–2652 (2012). [PubMed: 22323543]
32. Wang G et al. IRF4 ablation in B cells abrogates allogeneic B cell responses and prevents chronic transplant rejection. J. Heart Lung Transpl. 40, 1122–1132 (2021).
33. Miyahara Y et al. Anti-TCRβ mAb induces long-term allograft survival by reducing antigen-reactive T cells and sparing regulatory T cells. Am. J. Transplant. 12, 1409–1418 (2012). [PubMed: 22420295]
34. Chen S et al. Epigenetically modifying the Foxp3 locus for generation of stable antigen-specific Tregs as cellular therapeutics. Am. J. Transplant. 20, 2366–2379 (2020). [PubMed: 32167228]
35. Zhang HD et al. Ablation of interferon regulatory factor 4 in T cells induces 'memory' of transplant tolerance that is irreversible by immune checkpoint blockade. Am. J. Transplant. 19, 884–893 (2019). [PubMed: 30468559]

36. Zou D et al. T cell exhaustion is associated with antigen abundance and promotes transplant acceptance. Am. J. Transplant. 20, 2540–2550 (2020). [PubMed: 32185888]
37. Grubin CE, Kovats S, deRoos P & Rudensky AY Deficient positive selection of CD4 T cells in mice displaying altered repertoires of MHC class II-bound self-peptides. Immunity 7, 197–208 (1997). [PubMed: 9285405]
38. Gearty SV et al. An autoimmune stem-like CD8 T cell population drives type 1 diabetes. Nature 602, 156–161 (2022). [PubMed: 34847567]
39. Di Pilato M et al. CXCR6 positions cytotoxic T cells to receive critical survival signals in the tumor microenvironment. Cell 184, 4512–4530 (2021). [PubMed: 34343496]
40. Ng SS et al. The NK cell granule protein NKG7 regulates cytotoxic granule exocytosis and inflammation. Nat. Immunol. 21, 1205–1218 (2020). [PubMed: 32839608]
41. Kim CH et al. Bonzo/CXCR6 expression defines type 1-polarized T-cell subsets with extralymphoid tissue homing potential. J. Clin. Invest. 107, 595–601 (2001). [PubMed: 11238560]
42. Rengarajan J et al. Interferon regulatory factor 4 (IRF4) interacts with NFATc2 to modulate interleukin 4 gene expression. J. Exp. Med. 195, 1003–1012 (2002). [PubMed: 11956291]
43. Li P et al. BATF-JUN is critical for IRF4-mediated transcription in T cells. Nature 490, 543–546 (2012). [PubMed: 22992523]
44. Bettelli E et al. Reciprocal developmental pathways for the generation of pathogenic effector TH17 and regulatory T cells. Nature 441, 235–238 (2006). [PubMed: 16648838]
45. Lee Y et al. Induction and molecular signature of pathogenic TH17 cells. Nat. Immunol. 13, 991–999 (2012). [PubMed: 22961052]
46. Graef P et al. Serial transfer of single-cell-derived immunocompetence reveals stemness of CD8(+) central memory T cells. Immunity 41, 116–126 (2014). [PubMed: 25035956]
47. Aronoff L, Epelman S & Clemente-Casares X Isolation and identification of extravascular immune cells of the heart. J. Vis. Exp. 23, 58114 (2018).
48. Stuart T et al. Comprehensive integration of single-cell data. Cell 177, 1888–1902 (2019). [PubMed: 31178118]

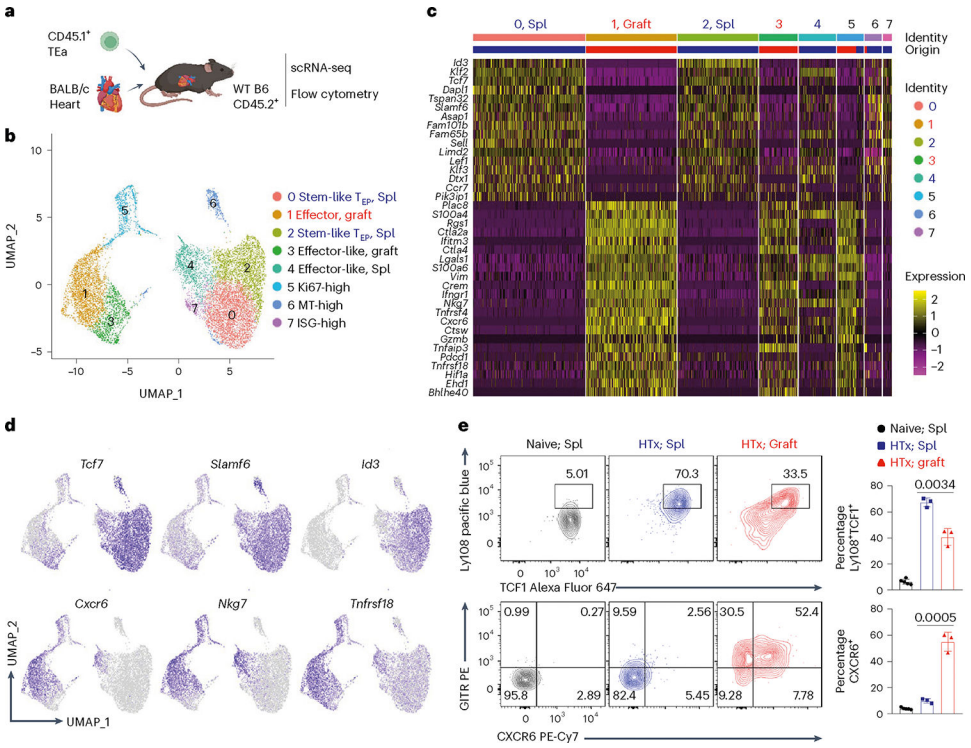

Fig. 1 |. Single-cell transcriptomics identifies alloimmune CD4$^+$ T_{EP} cells and effectors.

a–**e**, CD45.2$^+$ WT B6 mice were adoptively transferred with CD45.1$^+$ TEa transgenic CD4$^+$ T cells and transplanted with BALB/c hearts, followed by scRNA-seq and flow cytometric analyses of TEa cells at 7 d post-transplantation. Schematic of the experimental design (**a**). Created with BioRender.com. Uniform Manifold Approximation and Projection (UMAP) analysis of 10,964 single TEa cells from both spleens and allografts (**b**). Eight clusters (0–7) were identified and visualized with distinct color scheme. Heat map showing the expression of selected genes across all TEa cells (**c**). The top differentially expressed genes in the major T_{EP} cell clusters (0 and 2) versus the major effector cell cluster 1 are shown. The blue and red color bar indicates cell origin (blue, derived from spleens (Spl); and red, derived from grafts). Normalized expression of indicated genes projected onto the UMAP (**d**). Frequencies of Ly108$^+$TCF1$^+$ and CXCR6$^+$ cells among the transferred TEa cells in the spleens of B6 mice without transplantation (naive; Spl; $n = 5$ mice) or in the spleens (HTx; Spl) and the allografts (HTx; graft) of transplant recipients ($n = 3$ mice) (**e**). HTx, heart transplantation. Flow plots are gated on live TEa cells. Data are presented as mean ± s.d. (**e**). Results are representative of two independent experiments. *P* values are from a two-tailed unpaired Student's *t*-test.

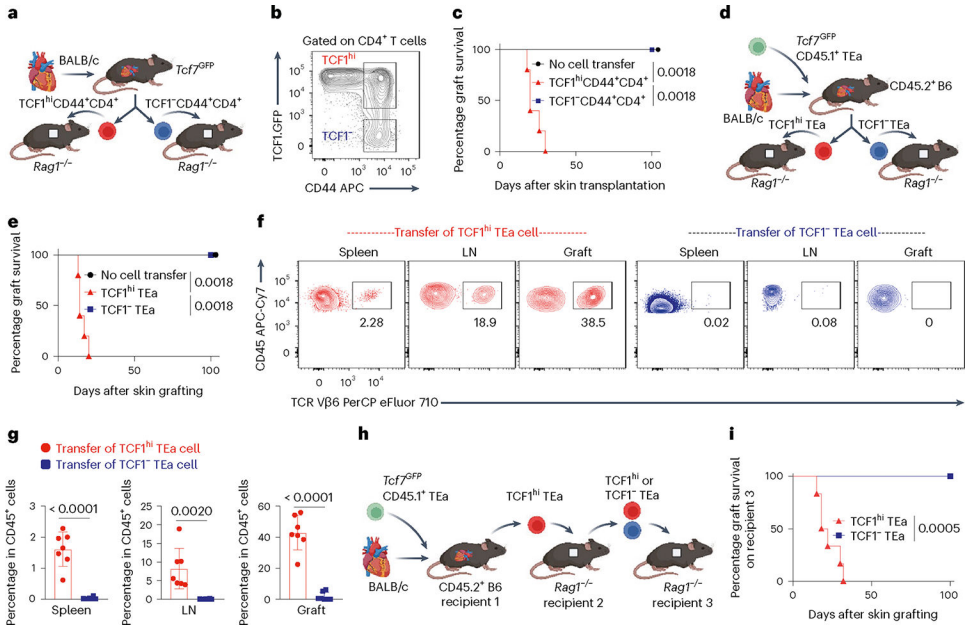

Fig. 2 |. Transfer of TCF1^{hi} CD4^{+} T$_{EP}$ cells but not TCF1^{-}CD4^{+} effector cells induces transplant rejection.

a–**c**, TCF1^{hi} or TCF1^{-}CD44^{+}CD4^{+} polyclonal T cells were sorted from the secondary lymphoid organs of *Tcf7*^{GFP} mice at 7 d post BALB/c heart transplantation, and adoptively transferred into *Rag1*$^{-/-}$ hosts that were transplanted with BALB/c skins 1 d later. Experimental scheme (**a**). Gating strategy for cell sorting (**b**). Percentage skin allograft survival. n = 5 mice per group (**c**). **d**–**g**, CD45.2^{+} B6 mice were adoptively transferred with CD45.1^{+} *Tcf7*^{GFP} TEa cells and transplanted with BALB/c hearts. TCF1^{hi} or TCF1^{-} TEa cells were isolated from the secondary lymphoid organs at 7 d post-heart transplantation, and adoptively transferred into *Rag1*$^{-/-}$ hosts that were transplanted with BALB/c skins 1 d later. Experimental scheme (**d**). Percentage skin allograft survival (**e**). n = 5 mice per group. Frequencies of the transferred TEa cells among CD45^{+} cells in *Rag1*$^{-/-}$ recipients at 21 d post-skin transplantation (**f**,**g**). Flow plots are gated on live CD45^{+} cells. n = 7 mice per group. **h**,**i**, *Tcf7*^{GFP} TEa cells were adoptively transferred into WT B6 mice (recipient 1) receiving BALB/c heart transplantation. TCF1^{hi} TEa cells from recipient 1 were transferred into *Rag1*$^{-/-}$ mice (recipient 2) receiving BALB/c skin transplantation. TCF1^{hi} and TCF1^{-} TEa cells from recipient 2 were transferred into new *Rag1*$^{-/-}$ hosts (recipient 3) receiving BALB/c skin transplantation. Experimental scheme (**h**). Percentage skin allograft survival on third recipients (**i**). n = 6 mice per group. Experimental schemes are created with BioRender.com (**a**,**d**,**h**). Data are presented as mean ± s.d. (**g**). Results are pooled from two independent experiments. P values are from a two-tailed unpaired Student's t-test (**g**) and log-rank test (**c**,**e**,**i**).

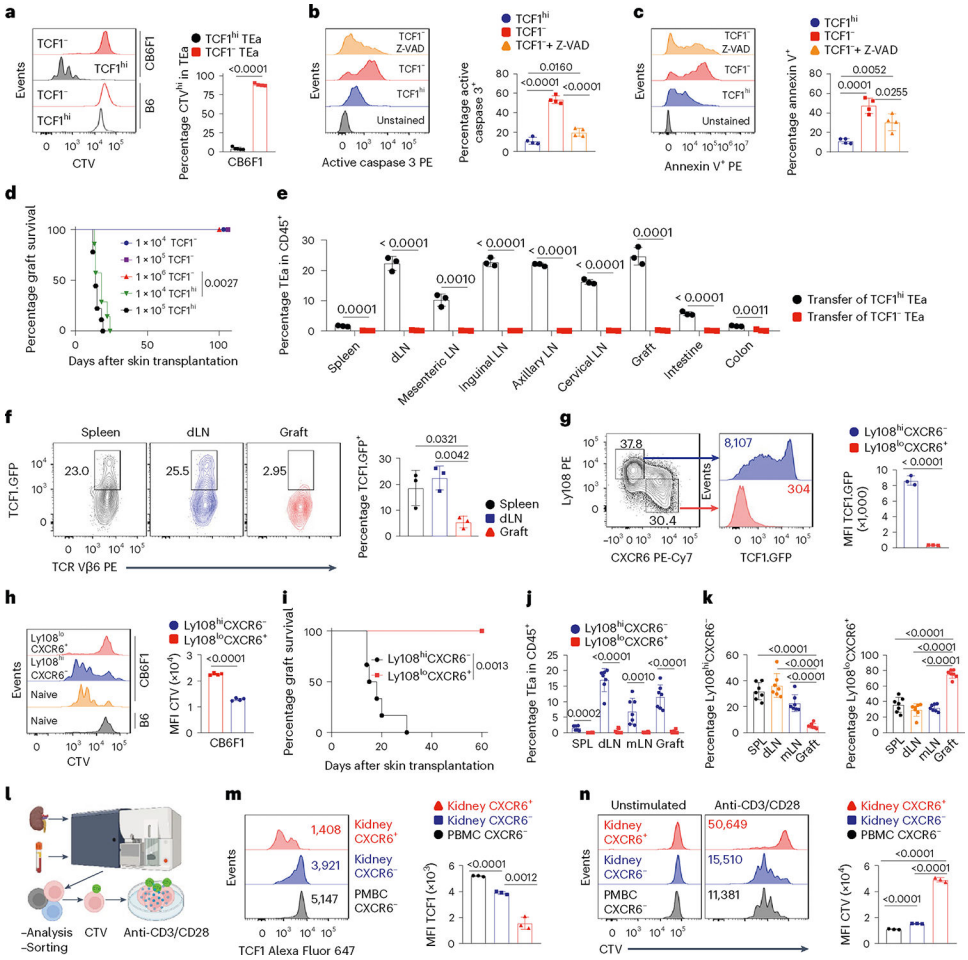

Fig. 3 |. CD4$^+$ T_{EP} cells function as reserve cells to replenish the effector cell pool.

a–**k**, CD45.1$^+$ *Tcf7*^{GFP} TEa cells were adoptively transferred into *Rag1*$^{-/-}$ mice receiving BALB/c skin transplantation. TCF1^{hi}, TCF1$^-$, Ly108^{hi}CXCR6$^-$ and Ly108^{lo}CXCR6$^+$ TEa cells were isolated from the secondary lymphoid organs at 14 d post-transplantation. Isolated TEa cells were either stimulated in vitro or adoptively transferred into new *Rag1*$^{-/-}$ hosts receiving BALB/c skin transplantation. Proliferation of CTV-labeled TCF1^{hi} or TCF1$^-$ TEa cells after in vitro stimulation with CB6F1 or B6 splenocytes (**a**). $n = 5$ biologically independent replicates for TCF1^{hi} TEa, and $n = 4$ for TCF1$^-$ TEa. Percentages of active caspase 3$^+$ (**b**) and annexin V$^+$ (**c**) in TCF1^{hi} and TCF1$^-$ TEa cells stimulated with CB6F1 splenocytes for 3 d, with or without 30 μM Z-VAD-FMK (Z-VAD) pan-caspase inhibition. $n = 4$ biologically independent replicates per group. In recipient mice transferred with TCF1^{hi} or TCF1$^-$ TEa cells, the graphs shown are percentage skin allograft survival (**d**; $n = 7$ mice for the 1×10^4 TCF1^{hi} group, and $n = 4$ mice for the 1×10^6 TCF1$^-$ group), frequencies of TEa cells among CD45$^+$ cells in indicated organs 14 d post-transplantation (**e**; $n = 3$ mice per group) and percentage of TCF1^{hi} cells derived from the transferred TCF1^{hi} TEa cells (**f**; $n = 3$ mice). dLN, draining lymph node. TCF1 expression in Ly108^{hi}CXCR6$^-$ and Ly108^{lo}CXCR6$^+$ TEa cells. $n = 3$ mice (**g**). MFI, mean fluorescence intensity. Proliferation of CTV-labeled Ly108^{hi}CXCR6$^-$, Ly108^{lo}CXCR6$^+$ or naive TEa cells after in vitro stimulation (**h**). $n = 4$ biologically independent replicates per group.

In recipient mice transferred with Ly108^{hi}CXCR6^{-} or Ly108^{lo}CXCR6^{+} TEa cells, the graphs shown are percentage skin allograft survival (**i**; $n = 6$ mice for the Ly108^{hi}CXCR6^{-} group and $n = 5$ mice for the Ly108^{lo}CXCR6^{+} group), frequencies of TEa cells at 14 d post-transplantation (**j**; $n = 7$ mice per group), and percentages Ly108^{hi}CXCR6^{-} and Ly108^{lo}CXCR6^{+} cells derived from the transferred Ly108^{hi}CXCR6^{-} TEa cells (**k**; $n = 7$ mice). mLN, mesenteric lymph node. **l**–**n**, CD4^{+} T cells from rejected human kidney allografts or PBMCs were analyzed by flow cytometry or cultured in vitro. Experimental scheme, created with BioRender.com (**l**). TCF1 expression in CXCR6^{-} and CXCR6^{+}CD4^{+} T cells (**m**). $n = 3$ biologically independent replicates. Proliferation of CTV-labeled CXCR6^{-} or CXCR6^{+}CD4^{+} T cells after stimulation with anti-CD3/anti-CD28 monoclonal antibodies (**n**). $n = 3$ biologically independent replicates per group. Data are presented as mean ± s.d. (**a**–**c**,**e**–**h**,**j**,**k**,**m**,**n**). Results are representative of two or three independent experiments (**a**–**c**,**e**–**h**) or pooled from two independent experiments (**j**,**k**). *P* values are from a two-tailed unpaired Student's *t*-test (**a**–**c**,**e**–**h**,**j**,**k**,**m**,**n**) and log-rank test (**d**,**i**).

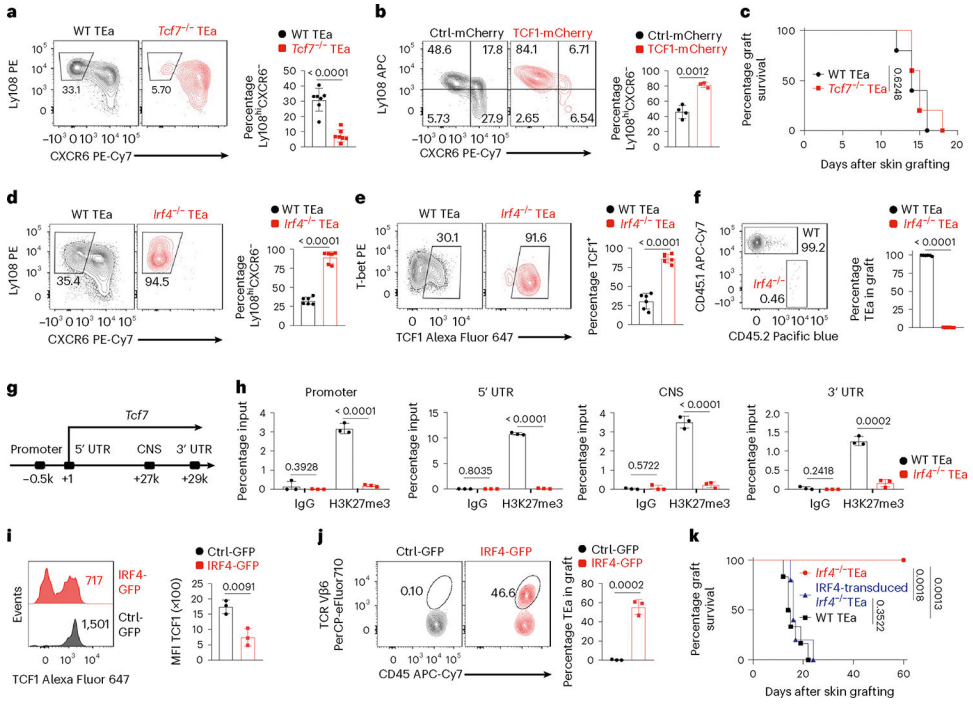

Fig. 4 |. TCF1 and IRF4 control distinct stem-like features of CD4$^+$ T$_{EP}$ cells.

a–**k**, *Rag1*$^{-/-}$ recipient mice were adoptively transferred with indicated TEa cell populations 1 d before BALB/c skin transplantation. TEa cells in spleens (**a**,**b**,**d**,**e**,**h**,**i**) and allografts (**f**,**j**) were analyzed at 14 d post-transplantation. Percentages of Ly108^{hi}CXCR6$^-$ cells derived from the co-transferred WT TEa and *Tcf7*$^{-/-}$ TEa cells (**a**). *n* = 7 mice. Percentages of Ly108^{hi}CXCR6$^-$ cells derived from the transferred WT TEa cells transduced with mCherry alone (Ctrl-mCherry) or TCF1-mCherry (**b**). Flow plots are gated on mCherry$^+$ TEa cells. *n* = 4 mice for the Ctrl-mCherry group and *n* = 3 mice for the TCF1-mCherry group. Skin allograft survival in mice transferred with WT TEa or *Tcf7*$^{-/-}$ TEa cells. *n* = 5 mice per group (**c**). Percentages of Ly108^{hi}CXCR6$^-$ cells derived from the co-transferred WT TEa and *Irf4*$^{-/-}$ TEa cells (**d**). *n* = 6 mice. Percentages of TCF1^{hi} cells derived from the co-transferred WT TEa and *Irf4*$^{-/-}$ TEa cells. *n* = 6 mice (**e**). Percentages of WT TEa and *Irf4*$^{-/-}$ TEa cells among total TEa cells in allografts (**f**). *n* = 6 mice. Chromatin immunoprecipitation (ChIP) analysis of H3K27me3 at the indicated regions of the *Tcf7* locus in WT TEa and *Irf4*$^{-/-}$ TEa cells (**g**,**h**). UTR, untranslated region. *n* = 3 biologically independent replicates per group. TCF1 expression in the transferred *Irf4*$^{-/-}$ TEa cells transduced with green fluorescent protein (GFP) alone (Ctrl–GFP) or IRF4–GFP. *n* = 3 mice per group (**i**). Percentages of the transferred *Irf4*$^{-/-}$ TEa cells (Ctrl–GFP or IRF4–GFP transduced) among CD45$^+$ cells in allografts (**j**). Flow plots are gated on CD45$^+$ cells. *n* = 3 mice per group. Skin allograft survival in groups transferred with WT TEa (*n* = 6 mice), *Irf4*$^{-/-}$ TEa (*n* = 5 mice) or IRF4–GFP transduced *Irf4*$^{-/-}$ TEa cells (*n* = 5 mice) (**k**). Data are presented as mean ± s.d. (**a**,**b**,**d**–**f**,**h**–**j**). Results are pooled from two independent experiments (**a**,**d**–**f**). Results are representative of two independent experiments (**b**,**h**–**j**). *P* values are from a two-tailed unpaired Student's *t*-test (**a**,**b**,**d**–**f**,**h**–**j**) and log-rank test (**c**,**k**).

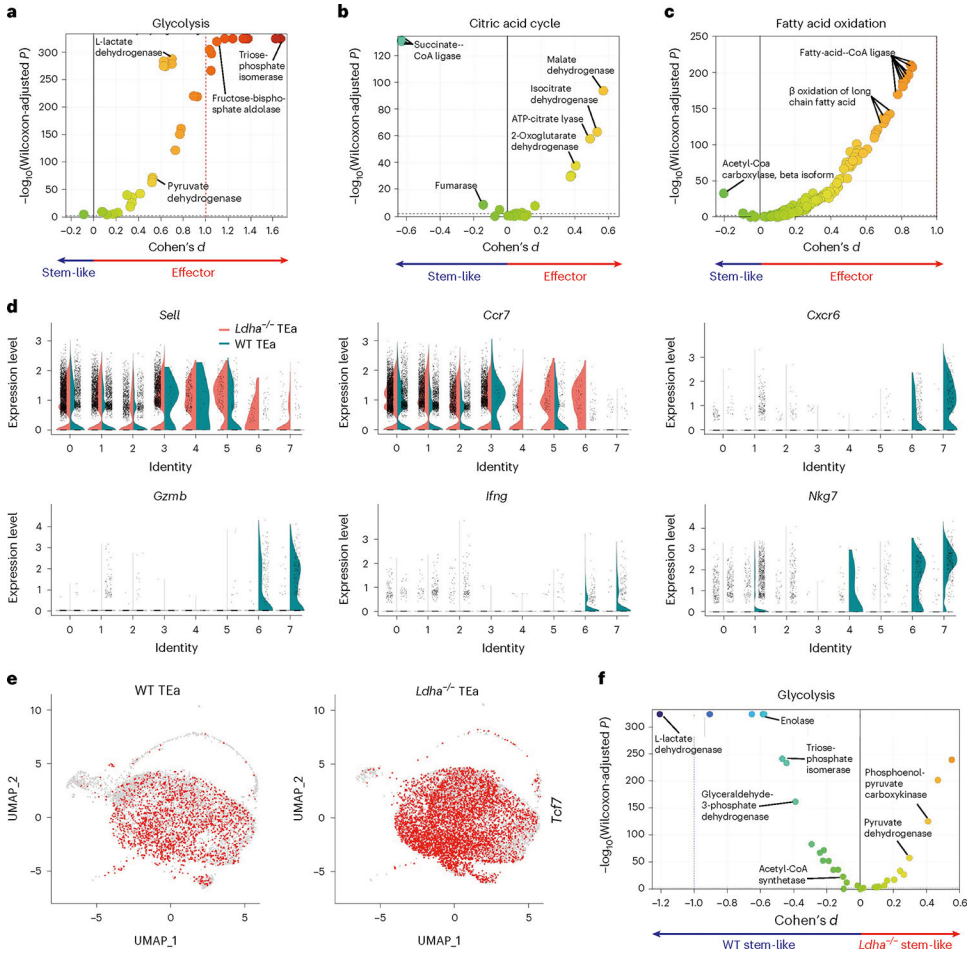

Fig. 5 |. scRNA-seq identifies LDHA as a crucial regulator of effector differentiation of T_{EP} cells. **a**–**c**, Compass algorithm was applied to determine the metabolic states of stem-like TEa cells and effector TEa cells, based on scRNA-seq data. Volcano plots illustrate the detailed *P* values and effect sizes for metabolic reactions in glycolysis (**a**), citric acid cycle (**b**) and fatty acid oxidation (**c**). **d**–**f**, scRNA-seq analysis of transferred WT TEa and *Ldha*$^{-/-}$ TEa cells, isolated from the spleens of heart transplant recipients 7 d post-transplantation. Split violin plots display the expression distributions of indicated stem-like genes and effector genes within each TEa cell cluster (**d**). The *Ldha*$^{-/-}$ and WT TEa cell populations are represented in red and green, respectively. Feature plots display the normalized *Tcf7* expression in WT TEa and *Ldha*$^{-/-}$ TEa cells, projected onto the UMAP (**e**). The volcano plot illustrates the detailed *P* values and effect sizes for metabolic reactions within the glycolysis subsystem, comparing WT stem-like TEa and *Ldha*$^{-/-}$ stem-like TEa cells, analyzed by Compass algorithm (**f**). Data were analyzed by two-sided Wilcoxon rank-sum tests with Benjamini–Hochberg correction for multiple comparisons (**a**–**c**,**f**).

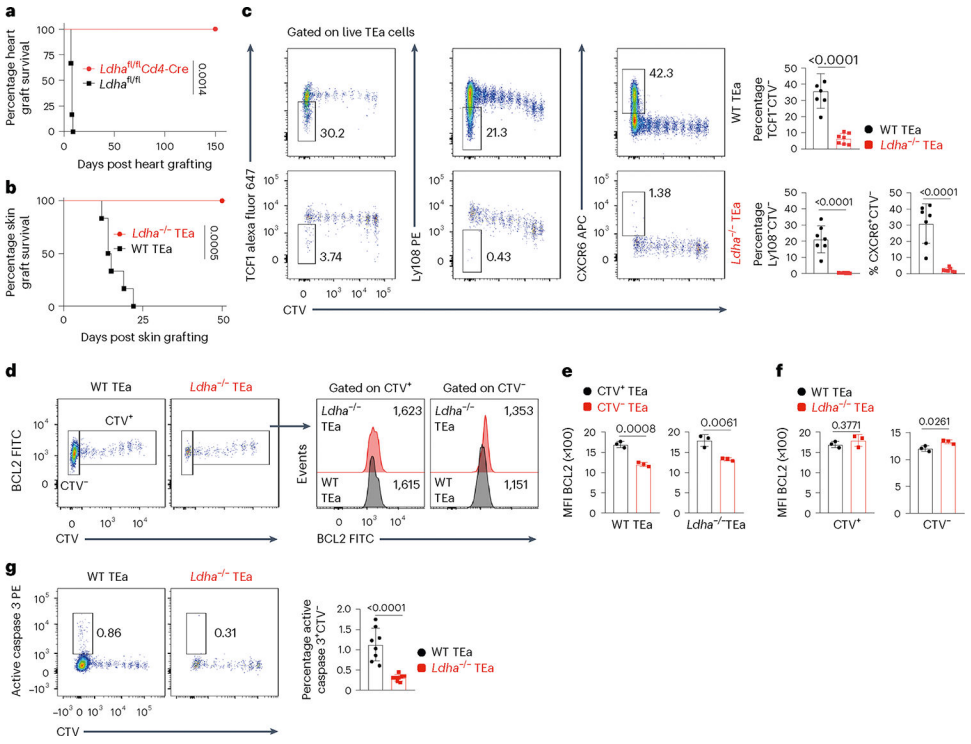

Fig. 6 |. LDHA governs the effector differentiation potential of CD4$^+$ T_{EP} cells.
a, Percentage BALB/c heart allograft survival in *Ldha*$^{fl/fl}$*Cd4*-Cre (n = 5 mice) or *Ldha*$^{fl/fl}$ control mice (n = 6 mice). **b**, Percentage BALB/c skin allograft survival on *Rag1*$^{-/-}$ mice transferred with *Ldha*$^{-/-}$ TEa or WT TEa cells. n = 6 mice per group. **c**–**g**, CD45.1$^+$ WT TEa and CD45.2$^+$ *Ldha*$^{-/-}$ TEa cells were mixed in a 1:1 ratio, labeled with CTV, and adoptively co-transferred into *Rag1*$^{-/-}$ mice 1 d before BALB/c skin transplantation. The transferred TEa cells were analyzed by flow cytometry on day 14 after skin transplantation. Representative flow plots and bar graphs show % TCF1$^-$CTV$^-$, Ly108$^-$CTV$^-$ and CXCR6$^+$CTV$^-$ TEa cells among the co-transferred WT and *Ldha*$^{-/-}$ TEa cells (**c**). n = 7 mice. Flow plots illustrate the gating strategy for CTV$^+$ and CTV$^-$ TEa cell populations and BCL2 expression within these populations (**d**). BCL2 expression levels in WT TEa or *Ldha*$^{-/-}$ TEa cells, comparing CTV$^+$ with CTV$^-$ cells. n = 3 mice (**e**). BCL2 expression levels in CTV$^+$ or CTV$^-$ cells, comparing WT TEa with *Ldha*$^{-/-}$ TEa cells (**f**). n = 3 mice. Flow plots and bar graphs show % CTV$^-$ active caspase 3$^+$ TEa cells among WT TEa or *Ldha*$^{-/-}$ TEa cells (**g**). n = 8 mice. Data are presented as mean ± s.d. (**c**,**e**–**g**). Results are pooled from two independent experiments (**c**,**g**) or are representative of three independent experiments (**e**,**f**). P values are from a two-tailed unpaired Student's t-test (**c**,**e**–**g**) and log-rank test (**a**,**b**).